UNCLASSIFIED
SECURITY CLASSIFICATION OF THIS PAGE

REPORT DOCUMENTATION PAGE

Form Approved
OMB No. 0704-0188

1a. REPORT SECURITY CLASSIFICATION	1b. RESTRICTIVE MARKINGS
2a. SECURITY CLASSIFICATION AUTHORITY	3. DISTRIBUTION/AVAILABILITY OF REPORT Approved for public release, distribution unlimited
2b. DECLASSIFICATION/DOWNGRADING SCHEDULE	
4. PERFORMING ORGANIZATION REPORT NUMBER(S)	5. MONITORING ORGANIZATION REPORT NUMBER(S) AFOSR-TR- 95 - 0355
6a. NAME OF PERFORMING ORGANIZATION: University of Washington 6b. OFFICE SYMBOL (If applicable)	7a. NAME OF MONITORING ORGANIZATION AFOSR/NA Bolling AFB DC 20332-6448
6c. ADDRESS (City, State, and ZIP Code) Seattle, WA 98195	7b. ADDRESS (City, State, and ZIP Code) AFOSR/NA Bolling AFB DC 20332-6448
8a. NAME OF FUNDING/SPONSORING ORGANIZATION Air Force Office of Scientific Research 8b. OFFICE SYMBOL (If applicable) NA	9. PROCUREMENT INSTRUMENT IDENTIFICATION NUMBER AFOSR-91-0195
8c. ADDRESS (City, State, and ZIP Code) AFOSR, 110 Duncan Avenue, Suite B 115 Bolling Air Force Base, DC 20332-0001	10. SOURCE OF FUNDING NUMBERS PROGRAM ELEMENT NO. 61102F; PROJECT NO. 2307; TASK NO. BS; WORK UNIT ACCESSION NO.

DTIC ELECTE MAY 24 1995 B

11. TITLE (Include Security Classification)
Program A-"The Effect of Rotational Motion on Jet-Impingement Cooling"
Program B-"The 'Tornado' Effect on Hairpin Vortices in Turbulent Convective Cooling"

12. PERSONAL AUTHOR(S)
M.Kurosaka

13a. TYPE OF REPORT	13b. TIME COVERED	14. DATE OF REPORT (Year, Month, Day)	15. PAGE COUNT
Final Technical Report	FROM 3/1991 TO 9/1994	December 31, 1994	

16. SUPPLEMENTARY NOTATION

17. GOSATI CODES			18. SUBJECT TERMS (Continue on reverse if necessary and identify by block number)
FIELD	GROUP	SUB-GROUP	VORTICES; FILMCOOLING;

19. ABSTRACT (Continue on reverse if necessary and identify by block number)

The overall objective of the program is to enhance the effectiveness of turbine cooling by exploiting the presence and structures of vortices.
Program A is concerned with jet impingement cooling and addresses the effects of bulk fluid rotation on jets, their vortical structures and cooling. A low-speed rotating water tunnel has been constructed for flow-visualization study of impinging jets in rotation: in addition, a rotating air rig was also constructed.The results show that the contour of the impinging jet is crucial in determining the jet trajectory and both the favorable and adverse effects of rotation have been identified in the context of impingement cooling.
Program B is concerned with convective and film-cooling. It focuses upon the so-called "tornado' effect, or the corewise transport of heat through the legs of hairpin vortices, which could lead to enhanced cooling in turbulent flows. An explicit confirmation of the effect have been established by ain water and unsteady heat transfer measurements in air.

20. DISTRIBUTION/AVAILABILITY OF ABSTRACT	21. ABSTRACT SECURITY CLASSIFICATION
☒ UNCLASSIFIED/UNLIMITED ☐ SAME AS RPT. ☐ DTIC USERS	UNCLASSIFIED
22a. NAME OF RESPONSIBLE INDIVIDUAL: DR JAMES MCMICHAEL	22b. TELEPHONE (Include Area Code): 202-767-4936 / 22c. OFFICE SYMBOL: AFOSR/NA

DD Form 1473, JUN 86 *Previous editions are obsolete.* SECURITY CLASSIFICATION OF THIS PAGE

DTIC QUALITY INSPECTED 5

UNCLASSIFIED

DISCLAIMER NOTICE

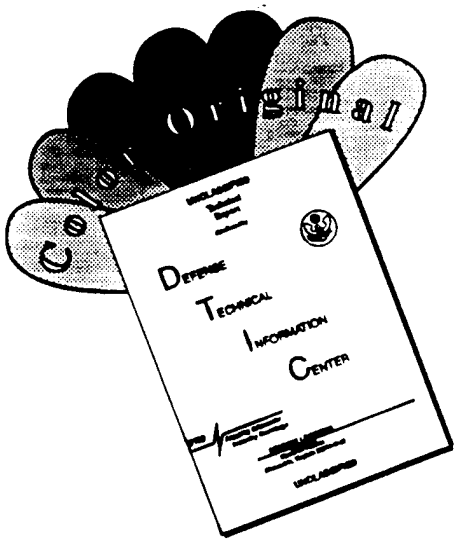

THIS DOCUMENT IS BEST QUALITY AVAILABLE. THE COPY FURNISHED TO DTIC CONTAINED A SIGNIFICANT NUMBER OF COLOR PAGES WHICH DO NOT REPRODUCE LEGIBLY ON BLACK AND WHITE MICROFICHE.

(1) Title:	program A-	"The Effect of Rotational Motion on Jet-Impingement Cooling"
	program B-	"The 'Tornado Effect' on Hairpin Vortices in Turbulent Convective Cooling"
(2) Overall Objective:		To enhance the cooling effectiveness of jet-impingement and convective cooling used in the hot turbine section of aircraft engines by exploiting the presence and motion of vortical structures.
(3) Grant Number:		AFOSR - 91-0195
(4) Principal Investigator and participating Graduate Students:		M. Kurosaka, P.I. and Professor; David C. Aronstein David W. Dartford, Michael D. Fox, Jeffrey P. Hagen, Stanley Hsu, Philippe C. Poutissou, and Stephen A. Whyte
(5) Organization and Address		Department of Aeronautics and Astronautics University of Washington Seattle, WA 98195
(6) Starting Date:		March 1, 1991
(7) Reporting Date:		March 1, 1991 to September 30, 1994

(8) Summary Description of the Entire Program

(8a) Air Force Needs

Compared to the present thrust-to-weight ratio of the current military aircraft engine, which is, for instance, about 6 for the F101, the far-term target in the year 2000 and beyond is aimed at values of 14-16, more than twice those achieved in the technology of today. As a key component improvement to push towards such a goal, the turbine temperature is envisioned to be raised from the current level of 2400 °F to 3600 °F. There-

(AFSC)
AIR FORCE
NOTICE
This
approved
Distribution
Joan
STINFO
reviewed and is
AFR 190-12
void.

19950523 050

fore, an increase of hot section cooling by 80% or more, without incurring any weight penalty, is considered to be an imperative.

(8b) Summary of Program A: "The Effect of Rotational Motion on Jet-Impingement Cooling"

In our proceeding AFOSR supported program, it has been demonstrated that vortex dynamics play a crucial role in impingement cooling schemes. Owing to the capacity of vortical structure to separate the total temperature, the cooling equivalent to 430 ^{o}F in the turbine thermal environment is found to be caused by the vortex rings in jets. These results are obtained in the setting of a non-rotating fluid. The rotation of the turbine blades, however, is expected to induce various first-order changes in the jet, its vortical structures, and their cooling effect. For instance, the trajectory of the impinging jet is expected to be strongly affected by rotation. Additionally, the Coriolis force may have a direct effect on, and deform the vortical structure in the jet, thereby altering the total temperature field. With these highlighting features in mind, we conduct a definitive, first-of-the-kind investigation to elucidate the effect of bulk-fluid rotation upon impingement cooling, a study expected to yield many counterintuitive physical phenomena.

(8c) Summary of Program B: "The 'Tornado Effect' of Hairpin Vortices on Turbulent Convective Cooling"

Program B is concerned with the central part of convective cooling, i.e., the heat transfer in transitional and turbulent boundary layers. Here we confine our attention to non-rotating fluids and focus on a flat plate with a transitional/turbulent boundary layer, which has two-dimensional mean flow and zero streamwise pressure gradient.

Approved for public release,
distribution unlimited

Within this framework, we address the following question: *What is the role of large-scale structures in turbulent heat transfer? How much of what has traditionally been ascribed to turbulent heat transfer is, in reality, attributable to large-scale structures? Would the augmentation of large-scale structures result in an increase in the turbulent heat transfer rate?*

The turbulent boundary layer is populated with large-scale arch-like hairpin vortices. A mechanism related to the hairpin vortices, which seems to have escaped attention in the past but is considered to have potent impact of heat transfer, appears to be at work: 'the tornado effect' or the crossflow transport of heat through the cores of the hairpin vortices .

Supporting evidence corroborative of the hypothesized mechanism is available. Chief among them is the fact that due to the directional preference of the tornado effect, *from the wall to the fluid,* the *direction* of the heat transfer -- either from the wall to the fluids or vice versa -- does make a difference in the magnitude of the heat transfer, this is contrary to the commonly held view.

This mechanism naturally suggests the intensification of hairpin vortices as a means to promote turbulent heat transfer. It is encouraging to note that sound has been found to increase the turbulent heat transfer by as much as 30%. This may be exploited favorably in the tone-rich environment of gas turbines.

Accession For	
NTIS GRA&I	☑
DTIC T&B	☐
Unannounced	☐
Justification	
By	
Distribution	
Availability Codes	
Dist	Avail and/or Special
A-1	

(9) Results

(9a) Program A

(9a-1) Flow Visualization

A full-scale rotating water rig, shown in Figure 1, was constructed for flow-visualization study (ref.1).

The large rotating water tank is 27" in diameter and 48" high. The maximum design speed of the tank is 200 rpm.The base and side wall are clear acrylic. The base rests on an aluminum turntable. An aluminum lid is bolted to the top of the side wall. The supply tank, valves, and other equipment are mounted on the aluminum lid. An opening at the center of the aluminum lid provides access to the tank. The tank interior is also accessible through a removable insert in the bottom of the tank, which is bolted in and sealed by an O-ring.

There is a stationary 30 gallon reservoir tank for preparing the jet fluid. Water is pumped from there into the on-board annular supply tank, and this can be done while the tank is rotating. The supply tank has a capacity of 600 in^3. The water level in the supply tank is typically 40 inches above the water level in the main tank. Flow is regulated by a plug-and-orifice valve similar to that in the pilot test rig. The plug is driven via a worm gear by an electric motor, and the position is indicated by a potentiometer. Electrical communication to the tank is accomplished via a 12-channel slip ring mounted on the centerline near the top of the supply tank. A pulsing valve is downstream of the main flow control valve. The jet pipe then extends into the test section, where it ends in a 1/2" diameter nozzle. The nozzle can be oriented at 0 degrees or 90 degrees to the rotation axis. With the nozzle parallel to the rotation axis, it is also on the centerline. A constant

water level in the main tank is maintained by a centrifugal drain. The drain pipe leaves the tank through a sealed opening in the aluminum lid, and exits into a non-rotating annular gutter. The end of the drain pipe is oriented such that the exit velocity of the water, as it leaves the drain pipe, is essentially canceled by the rotational motion of the drain pipe. This feature minimizes splashing. The gutter drains into a large dump tank.

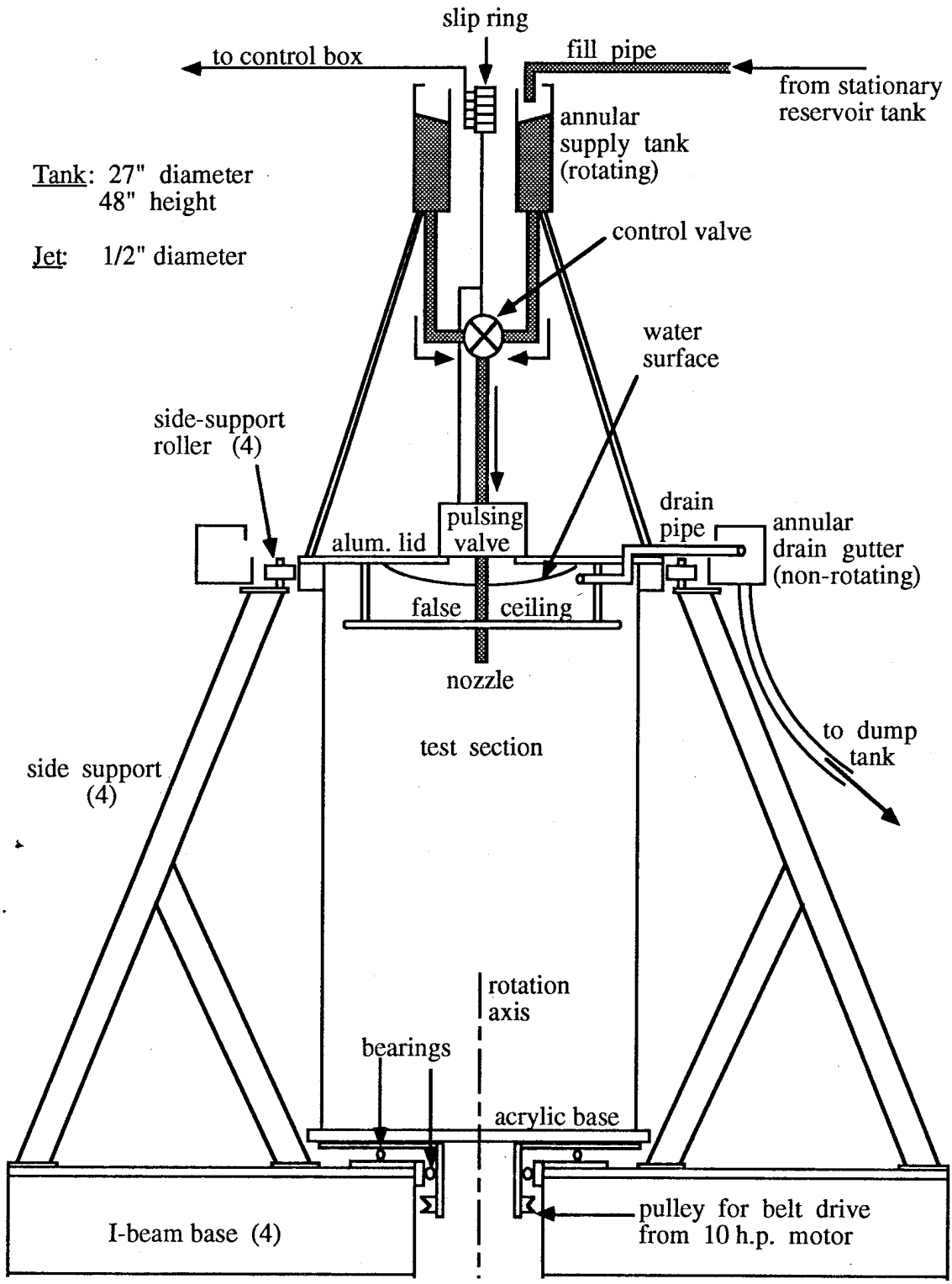

Figure 1. Rotating Water Tank.

(9a-1-1) Flow-visualization: Axial Jets

An axial jet is representative of the cooling near the leading edge of a turbine blade, where the direction of the jet is parallel to the rotational axis.

The rotating rig enabled us to identify gross features of a jet in rotation (ref.1), which appears to have important implications for practical applications. These features are related to the trajectories of jets; they embody a tendency of rotating fluids to resist any change in the direction along the axis of rotation, a fundamental property known as the Taylor-Proudman Theorem. Consider a flat impingement surface placed normal to the rotational axis (z axis); since on the plate the normal component of velocity (u_z) is zero (in inviscid flow), u_z everywhere tends to become zero. This tendency materializes in the unexpected behavior of jet trajectory.

Consider a jet discharged normal to such an impingement surface. The basic, non-rotating impingement flow is illustrated in Figure 2. For strong rotation (low Rossby number), the jet would fail to reach the surface for the reason stated above, unless the jet momentum is sufficiently large (flow-visualization of Figure 3 shows comparison between the two: non-rotating and strong-rotation). When the jet is sufficiently strong (high Rossby number), the near-field flow should be substantially unaffected by rotation. However, the importance of rotation rapidly comes into play as the flow spreads outward on the impingement plate. Simple continuity consideration suggest that the spreading velocity varies inversely with radial distance. So the effective local Rossby number, based on the radial distance, jet velocity and the rate of rotation, is inversely proportional to the square of the radial distance. Even at a high-Rossby number impinging jet is therefore expected to become rotation-dominated at some distance from the impingement point, as shown schematically in Figure 4. This is indeed verified and the

results are captured in video format.The radii at which the flow becomes rotation-dominated were made from the video images and their values denoted by Y (non-dimensionalized by the nozzle diameter d) is plotted in Figure 5 as a function of (global) Rossby number.

The suppression of axial jet velocities by the impingement plate appears to be detrimental to the cooling performance of such jets. At Rossby numbers below roughly 2, there is no jet in the conventional sense. The vortical structures which, in the absence of rotation, induce favorable total-temperature separation, are not present.

At higher Rossby numbers, the vortical structures are present in the jet and the impingement flow, out to a certain distance from the impingement point. Within this distance, enhanced cooling due to total-temperature separation may be expected. However, the radial extent over which favorable total-temperature separation can occur by vortices is limited by the effects of rotation. It is important to note that, even when the jet Rossby number is high, the far-field flow, having lower characteristic velocities and a larger length scale, will be characterized by a much lower Rossby number, and will therefore be strongly influenced by rotation.

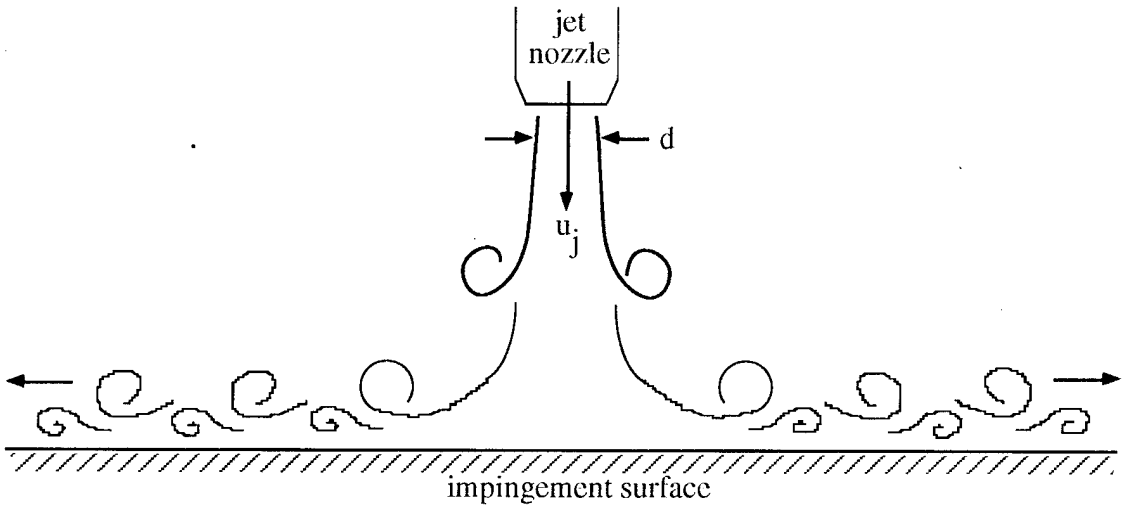

Figure 2. Impingement flow in the absence of rotation

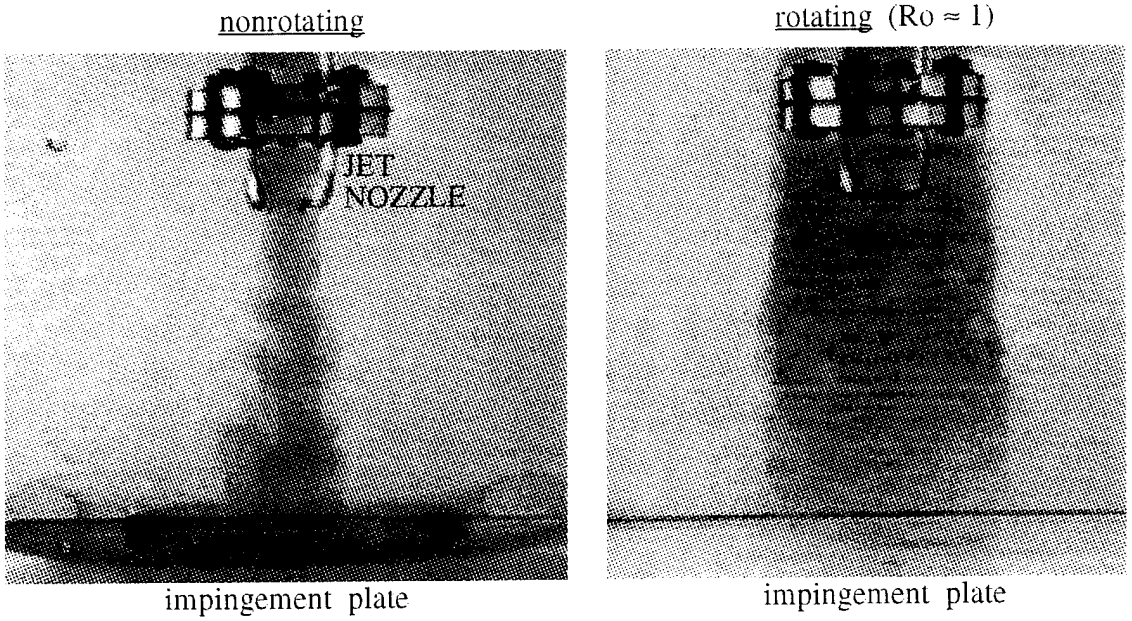

Figure 3. Axial jets without rotation (left) and with strong rotation (right)

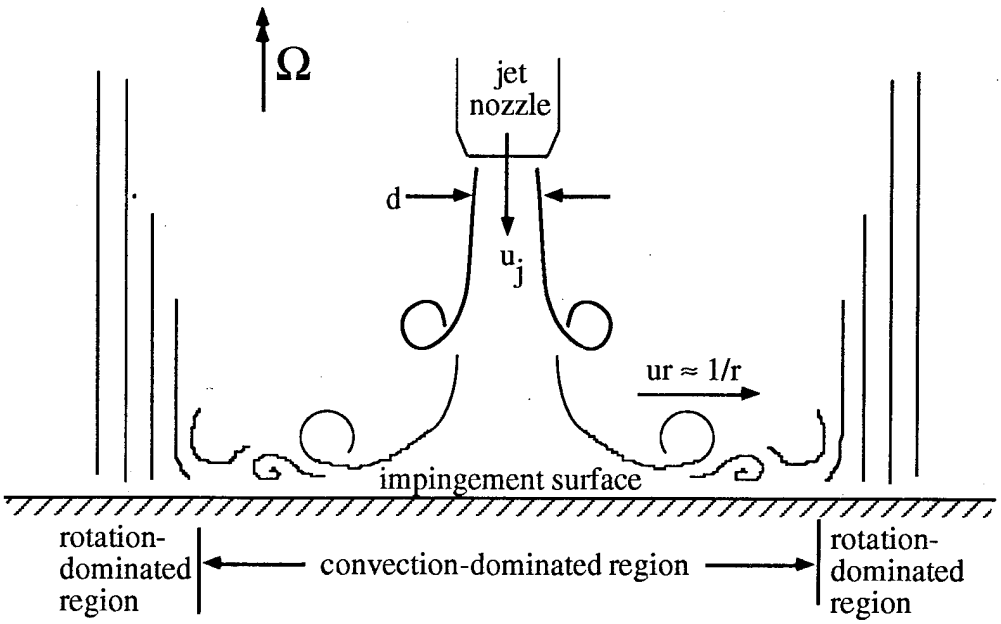

Figure 4. Impingement flow with moderate rotation.

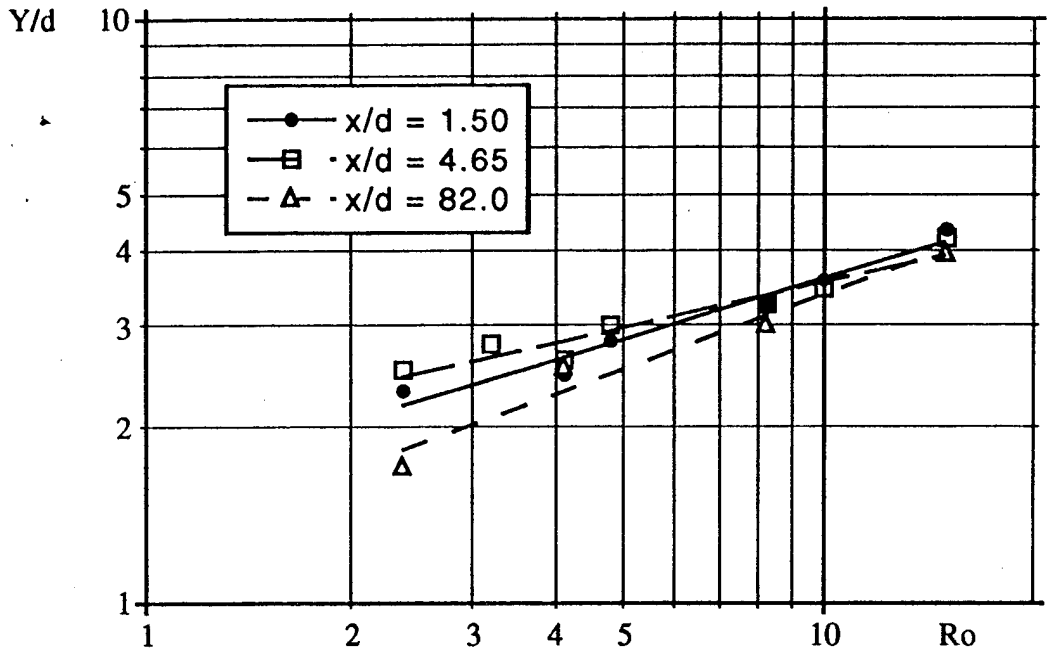

Figure 5. Radial extent vs. Rossby number

(9a-1-2) Flow-visualization:Transverse Jets

A transverse jet, in which the jet nozzle is approximately perpendicular to the axis of rotation, is typical of mid-chord impingement cooling. While not as critical as leading-edge cooling in terms of temperature, the mid-chord region does encompass a large portion of the blade surface; so it is important in terms of the amount of cooling flow devoted to it. Also, the heat transfer to the blade in this area may be quite high because the boundary layer on the outer surface of the blade is turbulent in the mid-chord region.

Of greater significance of rotation on a transverse jet is the effect of the aforementioned 2-dimensional tendency on a transverse jet (ref.1). The jet imposes a velocity u_j over a specific trajectory which lies at a specific value of z; the flow field tries to be 2-dimensional by matching that velocity at all values of z, above and below the jet trajectory. The result is that the jet pulls a "curtain" of fluid along with it, producing a planar jet even though the nozzle is axisymmetric.

As in the case of axial jets, the effect of a finite enclosure must be considered. At some distance away, in the axial direction, there must be an end wall with a no-flow-through boundary condition. Because $du/dz = 0$ everywhere, the end wall boundary condition is imposed on the entire flow field. Considering first the case of a jet at 90 degrees to the rotation axis, and a horizontal end wall, it can be seen that there is no conflict between the jet orientation and the boundary condition (Figure 6). However, if the jet direction does not match the end wall slope, there is a conflict, as shown in Figure 7. If the Rossby number is sufficiently low, the jet would be expected to follow the end wall boundary condition, *even if that boundary is many jet-diameters away from the nozzle.* If

it is intended to direct a jet at 45 degrees to the rotation axis, for example, it would seem necessary to slope the end wall at a similar angle as in Figure 8.

Observations of the formation of a planar jet, and of end-wall effects on the jet trajectory, were made. Dye in the jet fluid was used for flow visualization, and the camera was in the fixed frame of reference, positioned so as to give a side view of the flow. The Rossby number was approximately 1 in all cases. The flows corresponding to Figures 6 through 8 are shown in Figures 9 through 11, respectively. In the experimental runs shown in Figures 9 and 10, both upper and lower boundaries were flat. In Figure 11, the lower boundary was sloped, while the upper boundary was a free surface. The jet nozzle was located closer to the lower boundary to insure that the sloped boundary condition would be felt at the nozzle. The expected flow patterns were seen. That is, the jet entrained a vertical "curtain" of fluid within a very short distance from the nozzle. Furthermore, the flow followed the end-wall contour in each case. In the second case, where the jet was at 45 degrees to the axis and the end wall was normal to the axis, the boundary condition of the end wall prevailed.

In cases 1 and 2, the final distribution of jet fluid was centered at the same height as the jet nozzle, even though the nozzle was directed downward in case 2. Only in case 3 was the bulk of the jet fluid transported in the vertical direction.

If the boundary conditions conflict greatly, then the flow becomes less predictable. In ref. 2, it was observed that when the top and bottom boundary conditions are strongly different, a transverse jet follows the slope of the closer boundary. If the jet is roughly equidistant from the two boundaries, then it tends to follow one or the other, sometimes

fluctuating between the two, rather than assuming a steady direction equal to the average of the two end wall slopes.

Upon completion of a free transverse jet study, an investigation of impinging transverse jets was carried out. For the purpose of the present work, an impinging jet is considered to impact perpendicularly onto a flat surface. To accomplish this, jet path curvature due to Coriolis force must be correctly allowed for. Experimentally, steps were taken to insure that correct impingement was achieved. Figure 12 shows the experimental set up used for observation of impinging transverse jets.

Assuming the jet reaches the impingement plate while retaining its 3-dimensional character, the near-field impingement flow is expected to resemble that of a non-rotating jet, as shown previously in Figure 2. A schematic view of this flow, looking directly onto the impingement plate, is shown in Figure 13. The concentric circles denote vortex rings spreading radially on the impingement plate. As in the case of the impinging axial jet, rotation will become dominant at some point as the flow spreads and slows. The expected flow, exhibiting a transition from the non-rotating flow pattern to the rotation-dominated flow pattern, is shown schematically in Figure 14. Enhanced cooling due to total-temperature separation seems to be achievable under these conditions. Experiments

Figure 15 shows the details of experimental set up used for observation of impinging transverse jets. A false floor and backdrop, both white, were installed to aid in visualization. The impingement plate was clear, and a mirror was installed behind it to provide a view onto the plate, for the overhead on-board video camera. With the appropriate zoom setting on the camera, both a direct top view and the view onto the plate could be

observed simultaneously. This feature was useful in understanding the observed flow patterns. Phenolphthalein in the jet fluid was used as a dye, with base (NaOH) in the jet fluid and acid (HNO_3) in the ambient fluid. This made the jet fluid visible with high contrast for the extent of the impingement flow, but caused it to become clear upon mixing with the ambient fluid, so that the view of the test section was not obscured. The Rossby number range for impinging transverse jet experiments was 2.5 to 5, corresponding to a jet velocity of 5 inches per second and rotation rates of 20 to 40 revolutions per minute. The impingement plate was typically positioned 2 jet-diameters from the nozzle ($x/d = 2$).

As a basis for comparison, Figure 16 shows an impinging jet in the absence of rotation ($Ro = \infty$), in the present experimental set up. Radially spreading vortex rings are clearly visible in the view onto the impingement plate.

Figure 17 shows the typical impingement flow, at a Rossby number of 4.7. A radial pattern is seen up to a distance of about 2 jet-diameters from the impingement point. Columnar structures are seen outside of that region. An important feature of the flow is that the columnar vortices on the observer's left are continually moving along the plate, while *the single large columnar vortex on the right is stationary.* The asymmetric impingement flow, with a stationary vortex on one side, was entirely unexpected.

It was furthermore observed that the left-hand flow sometimes wrapped around the edge of the impingement plate, and even continued along the back surface (Figure 18). The right-hand flow, in every case in which it was visible, separated prior to reaching the edge of the plate.

When the jet impinges on the plate, a radially spreading wall jet is generated. As expected, the effect of rotation is to break this up into two plane wall jets, one proceeding to the right and one proceeding to the left. It is well known that a straight flow, transverse to the rotation axis, is only possible if there is a lateral pressure gradient to oppose the Coriolis force. The momentum equation, simplified for a steady, uniform, flow, gives

$$2\Omega \times U = -\frac{1}{\rho}\nabla p \quad .$$

The orientation of the vectors, and the sense of the required pressure gradient, are shown in Figure 19. Thus, in the right-hand flow, pressure must decrease as one proceeds from the outer fluid toward the plate; while the opposite must happen in the left-hand flow. For each case, the ambient pressure outside the wall jet is the same. So the right-hand wall jet has a region of low pressure along the plate, while the left-hand wall jet has a region of high pressure along the plate. Now consider what happens when each wall jet approaches its respective edge of the impingement plate. The ambient pressure is imposed beyond the edges of the plate, as shown in Figure 20. This causes a strong adverse pressure gradient for the right-hand flow, naturally leading to separation prior to reaching the plate edge. The separation point seems to position itself quite far inboard from the edge, i.e., close to the impingement point, leading to the observed stationary vortex. The left-hand flow experiences a strong favorable pressure gradient, accelerating it toward the edge of the plate, and sometimes even around the edge and up the other side.

The resulting flow, including the vortical structures generated by the jet, is shown in Figure 21. The left-hand flow has features which indicate effective cooling. The structures become columnar and sweep along the impingement plate for large distances, at

least 6 jet-diameters, which was the extent of the plate in the present experiment. Thus the entire left side (in the observer's view) of the plate would experience cooling by the jet, including the favorable total temperature separation. This possibly represents an improvement in cooling performance, over what can be achieved in the absence of rotation. However, the right-hand side of the plate suffers a twofold reduction in cooling effectiveness. First, the flow extends less than 3 jet-diameters from the impingement point in that direction before it separates. Second, even within that range, there would be no total temperature separation because the vortical structure is stationary.

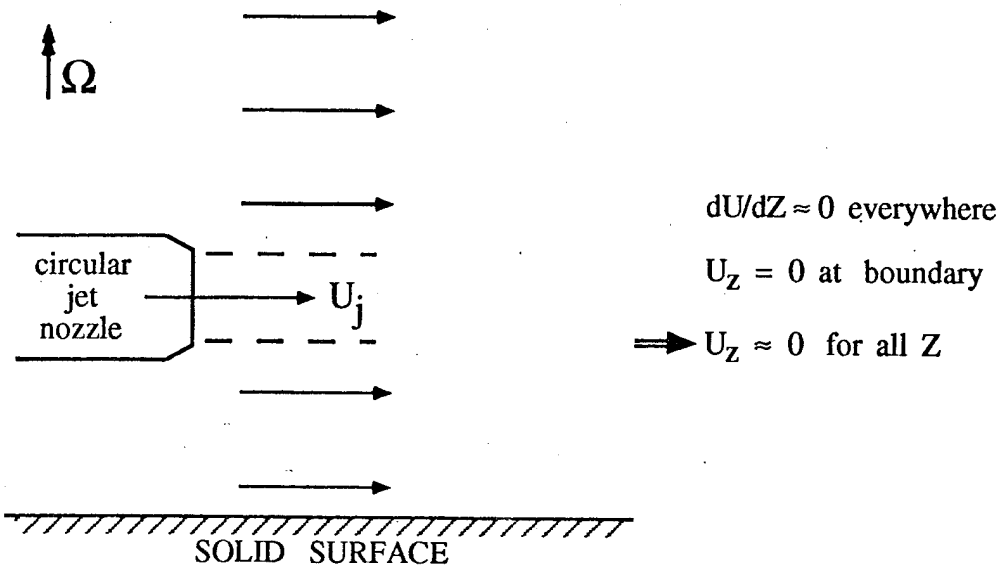

Figure 6. Horizontal jet with horizontal end wall.

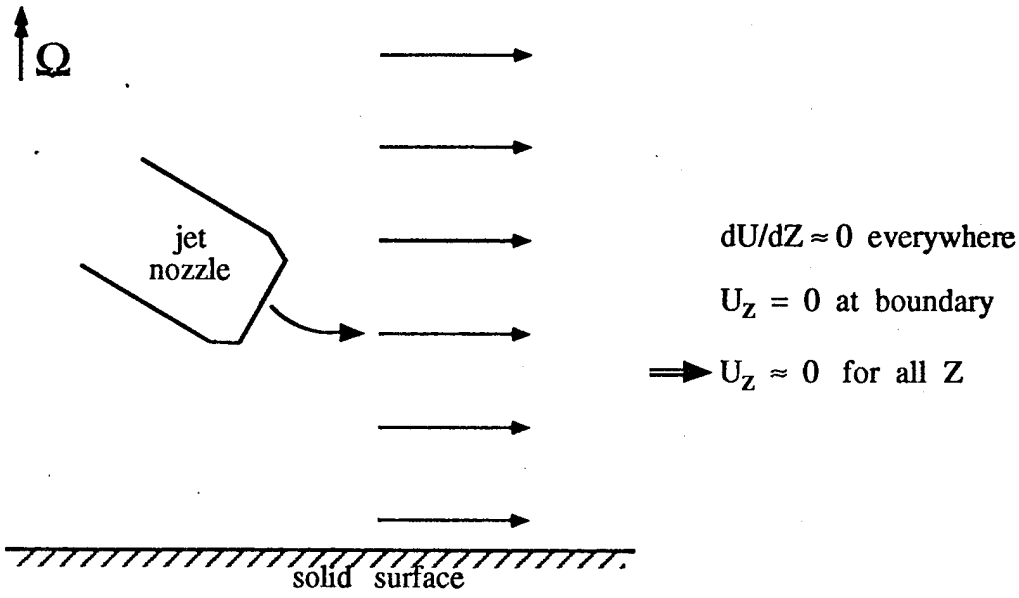

Figure 7. Oblique jet with horizontal end wall.

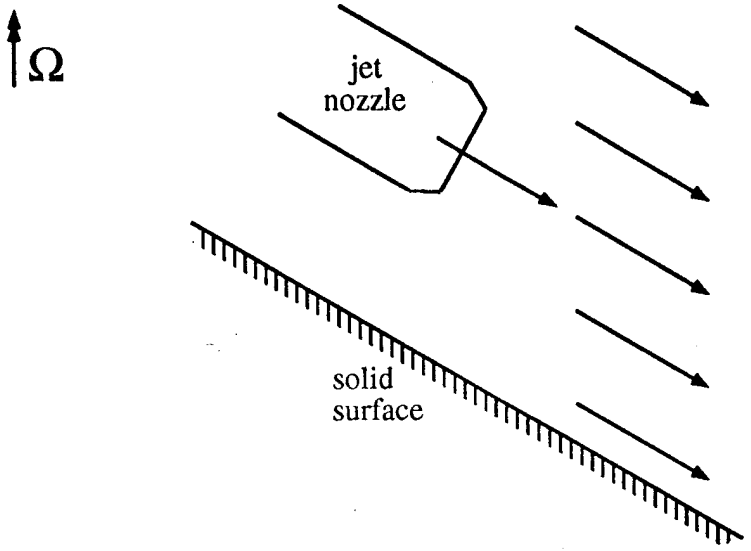

Figure 8. Oblique jet with matching sloped end wall.

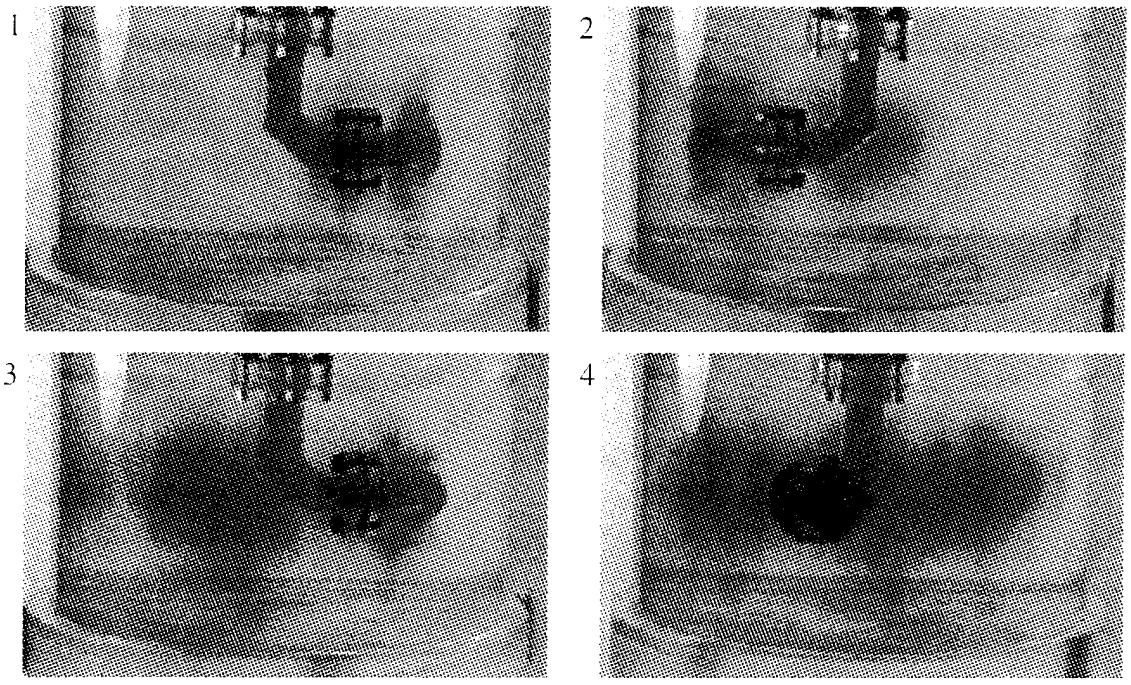

Figure 9. Case 1: Horizontal jet and horizontal end wall.

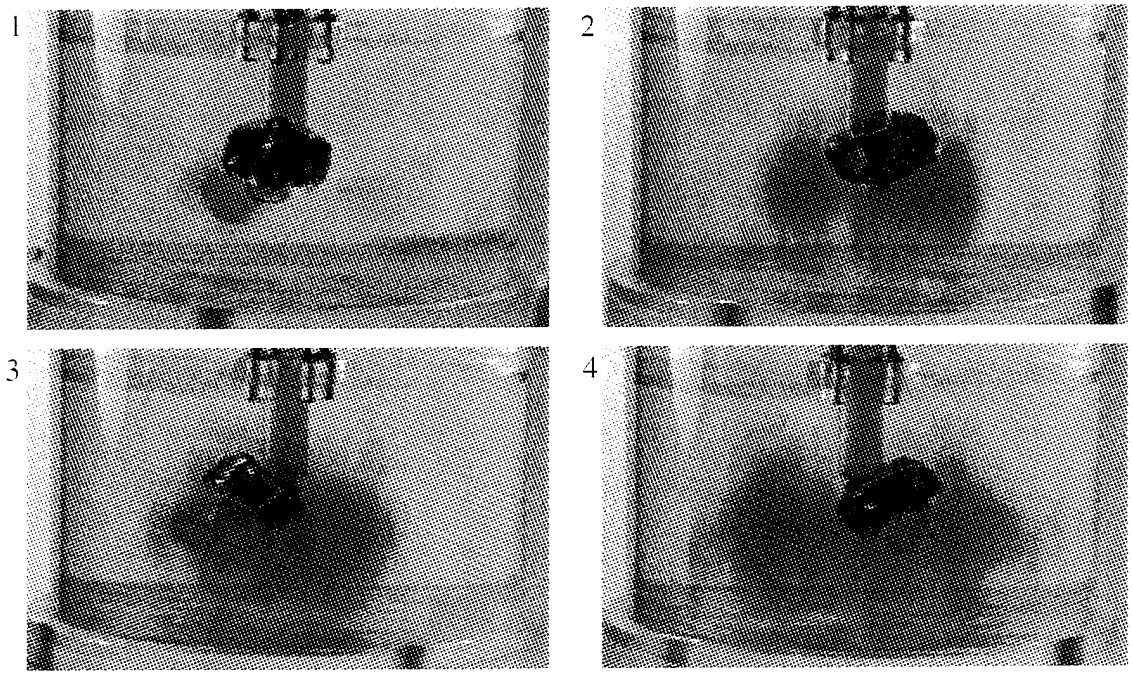

Figure 10. Case 2: Oblique jet and horizontal end wall.

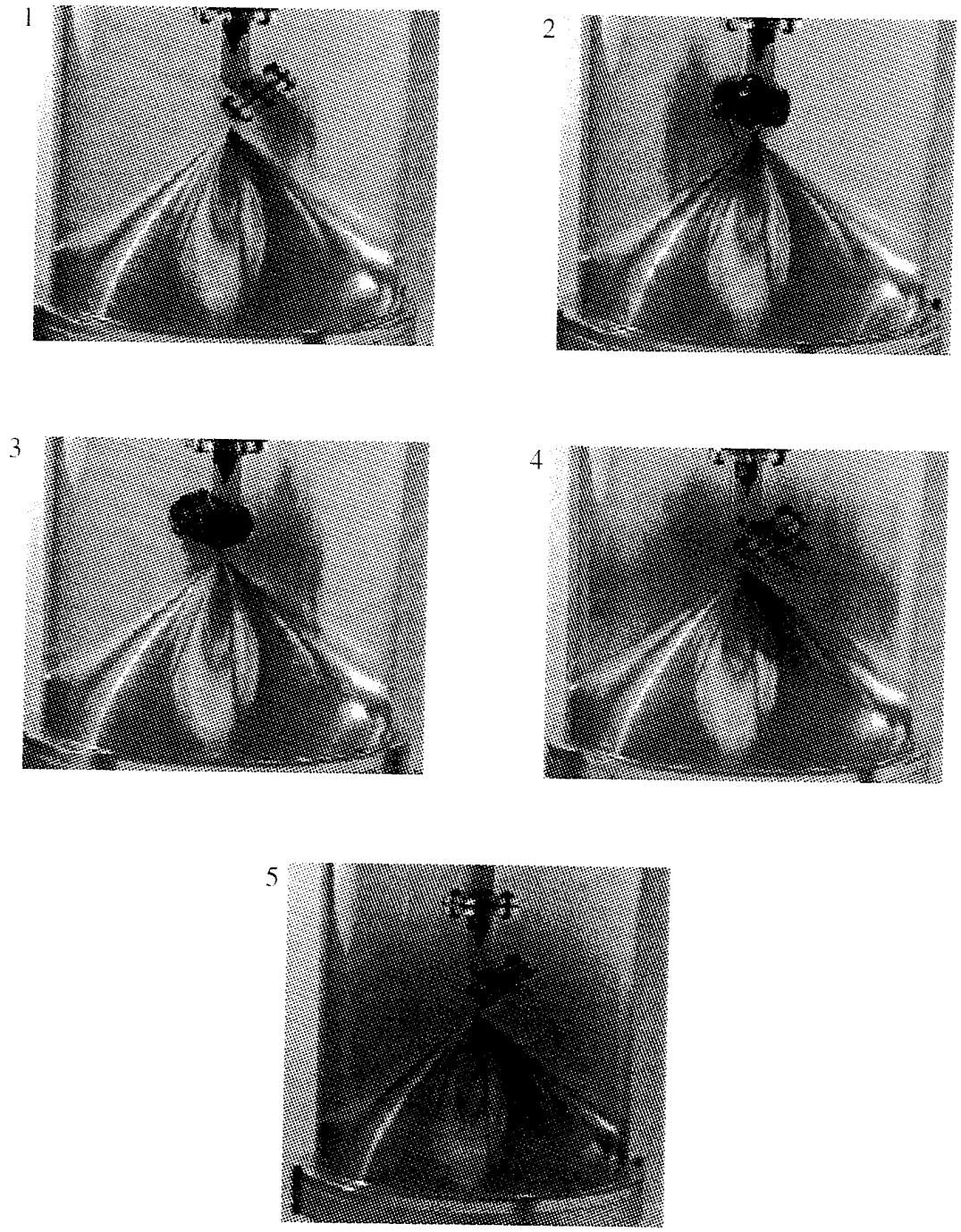

Figure 11. Case 3: Oblique jet with sloped end wall.

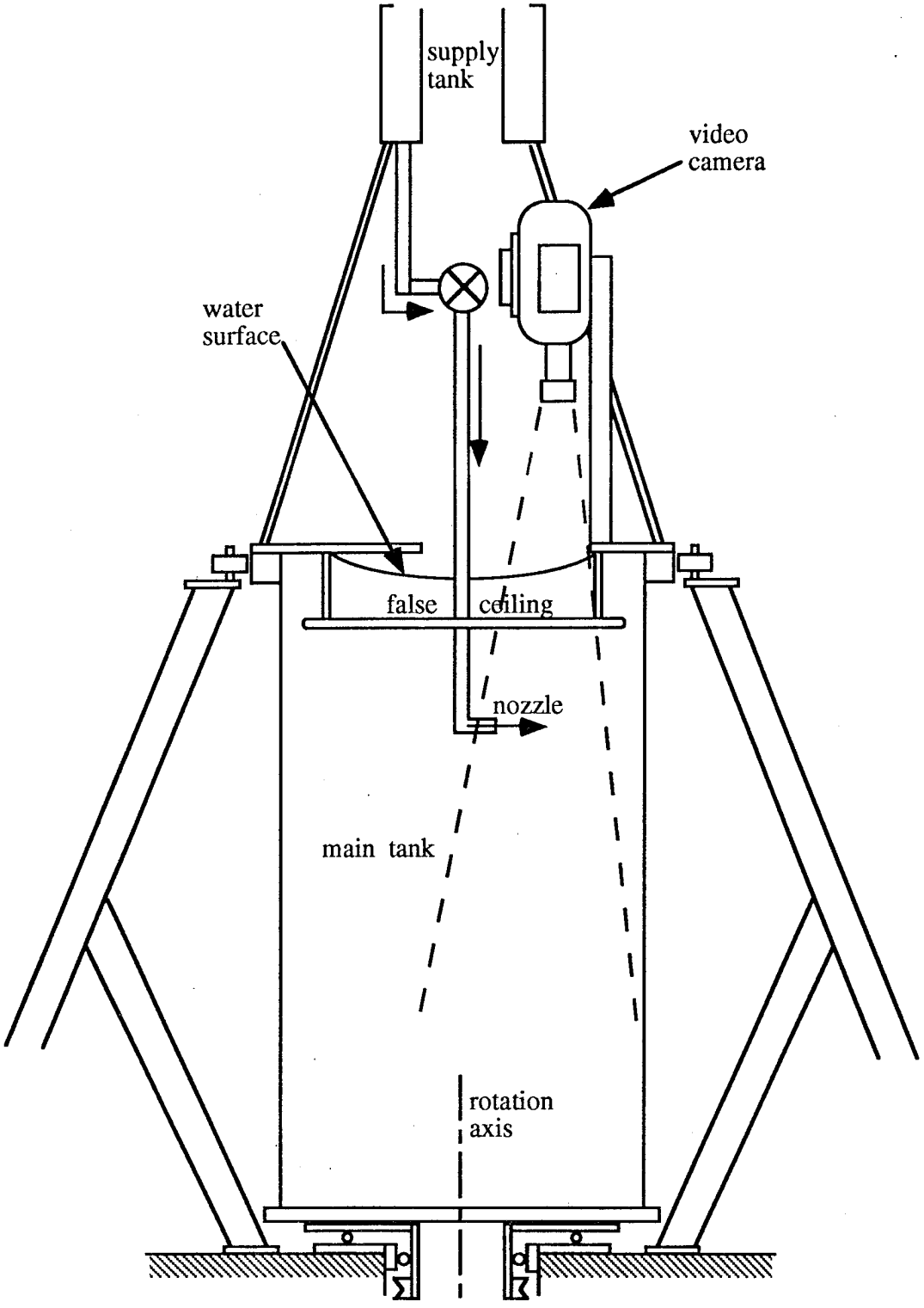

Figure 12. Experimental set up for observation of free transverse jets

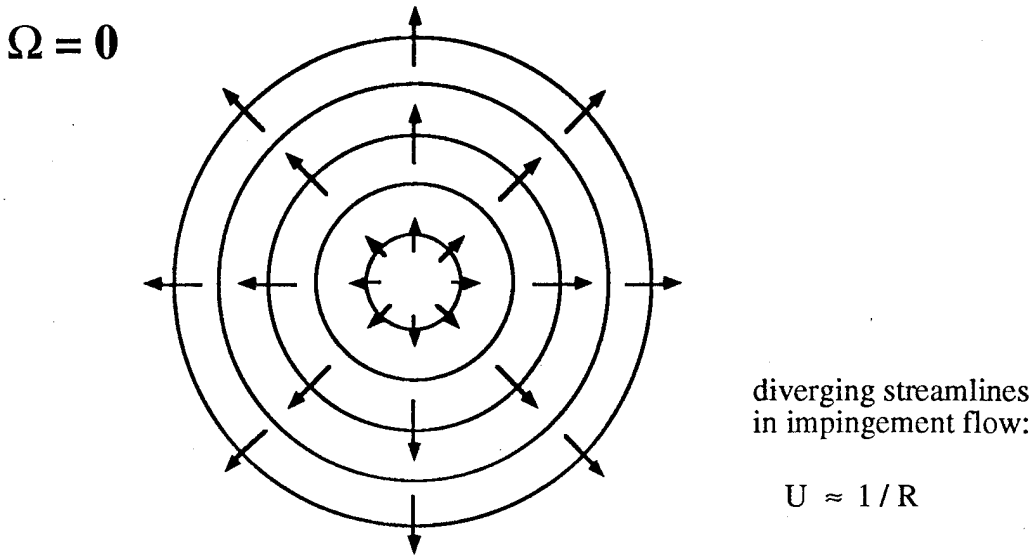

Figure 13. Non-rotating impingement flow: view onto the plate

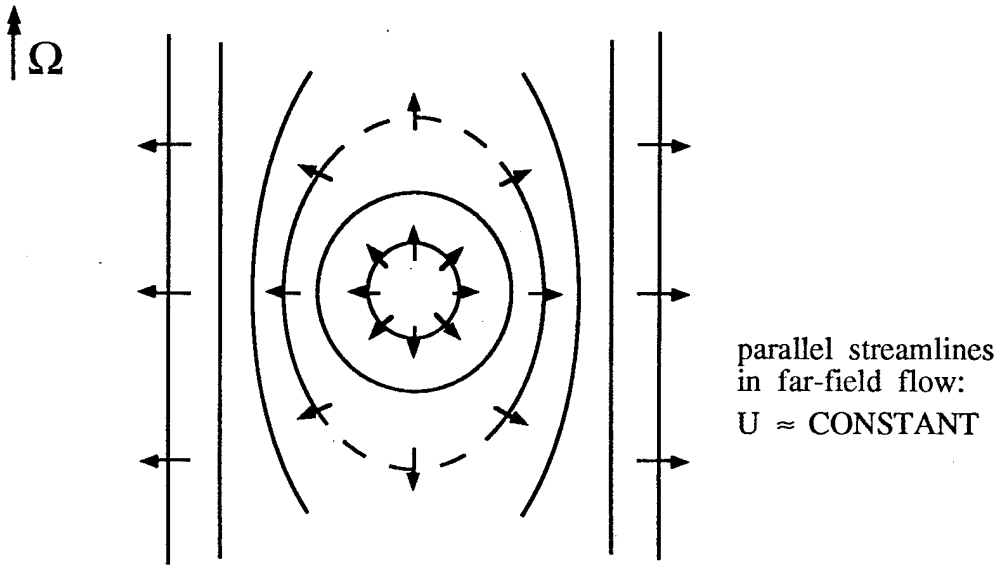

Figure 14. Expected rotating impingement flow: view onto the plate

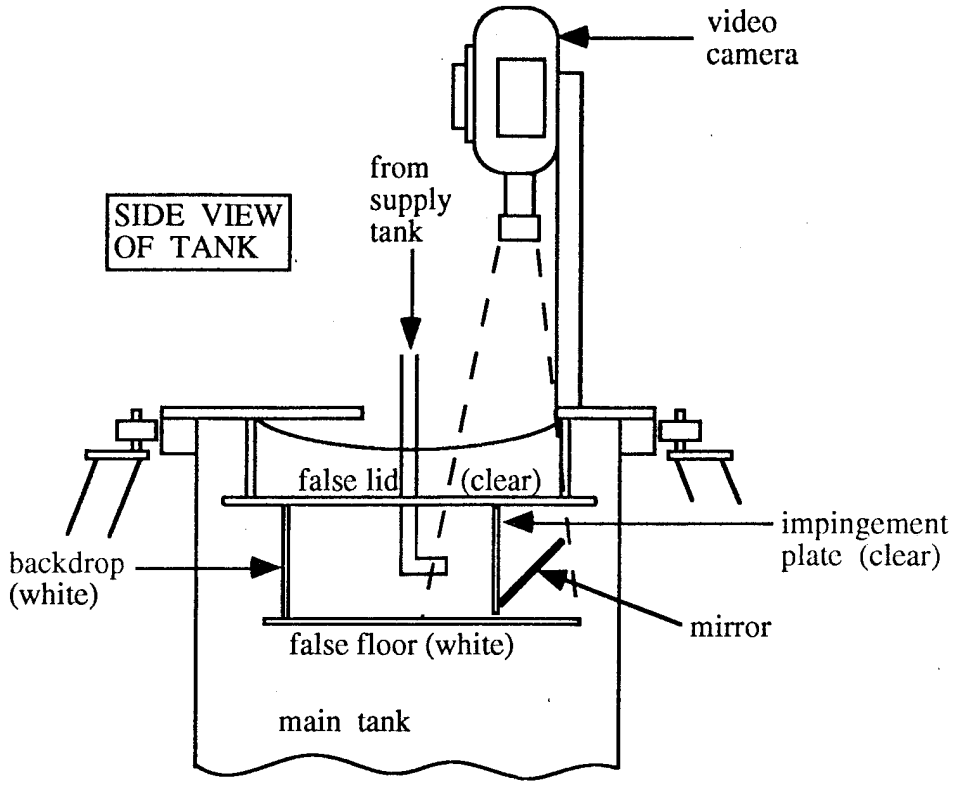

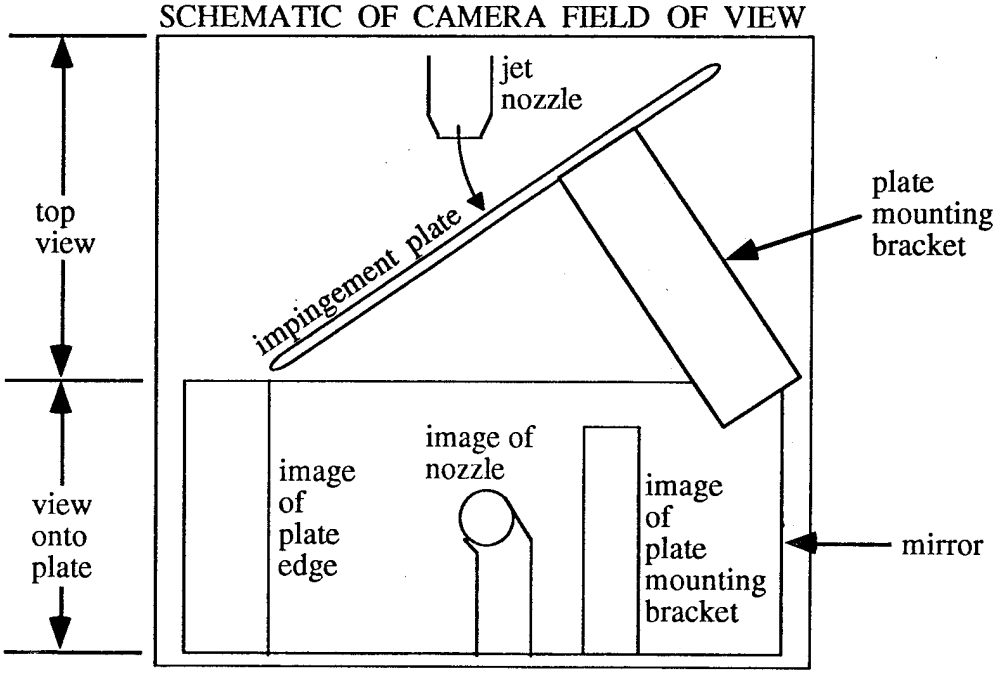

Figure 15. Experimental set up for impinging transverse jets

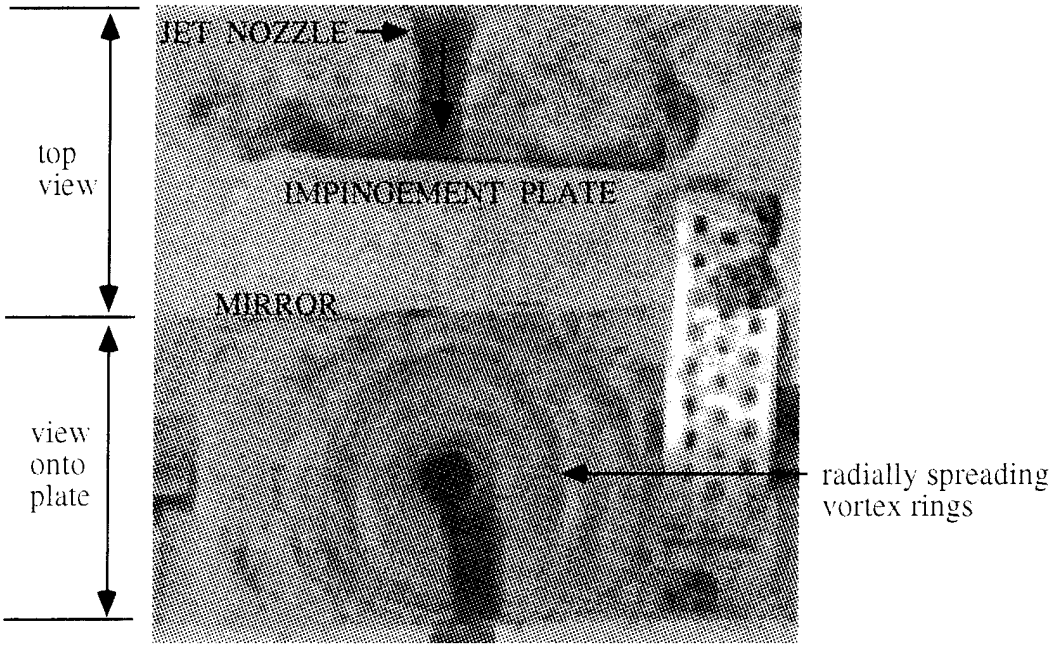

Figure 16. Impinging jet in the transverse set-up, non-rotating

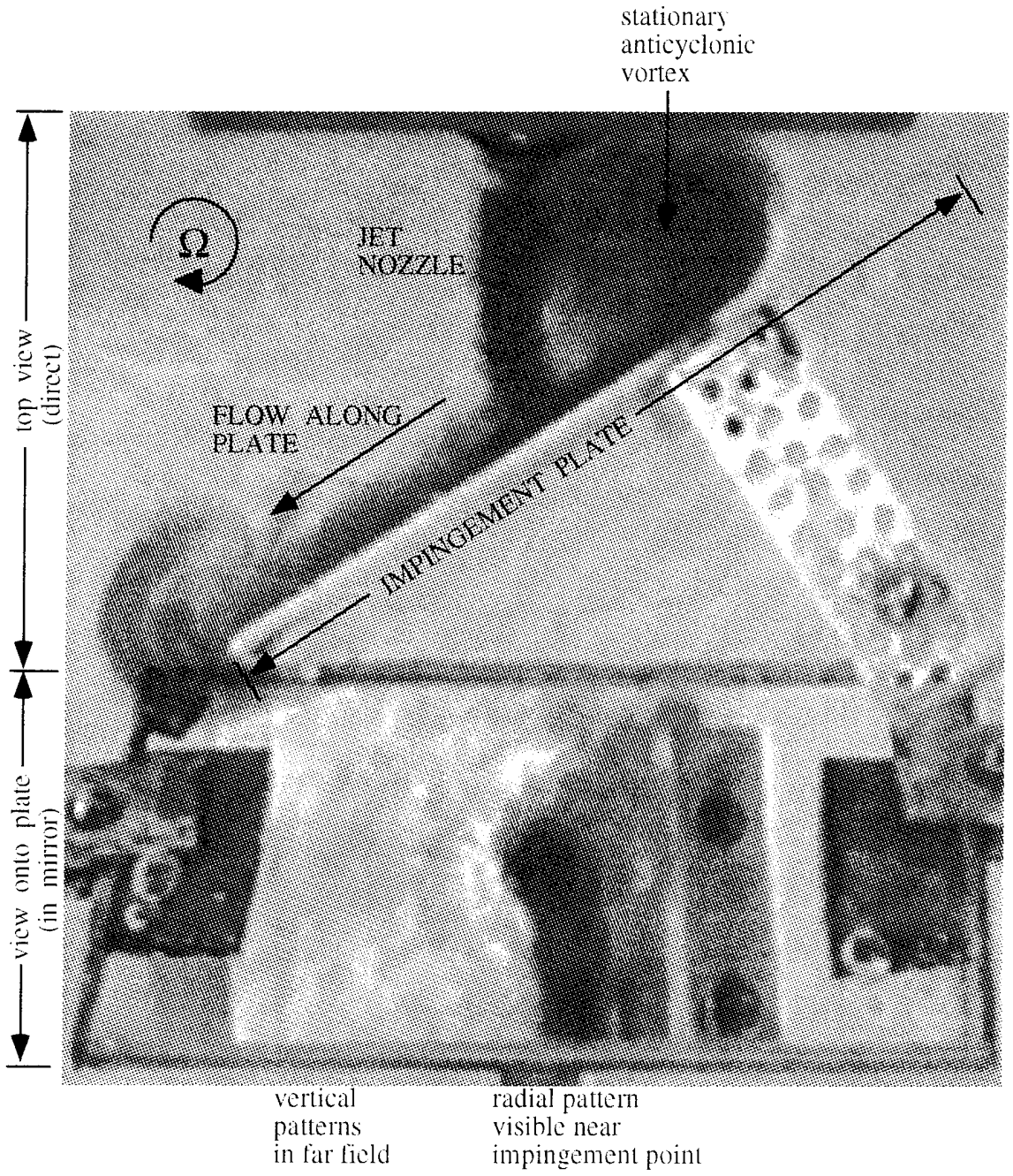

Figure 17. Impinging transverse jet

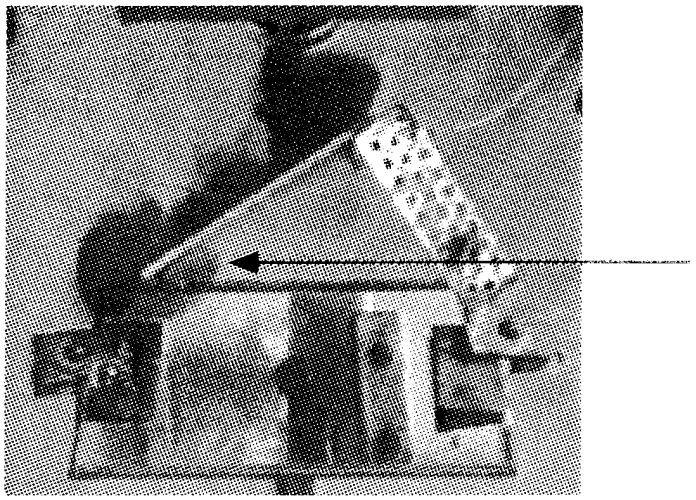

Figure 18. Left-hand flow wrapping around plate edge

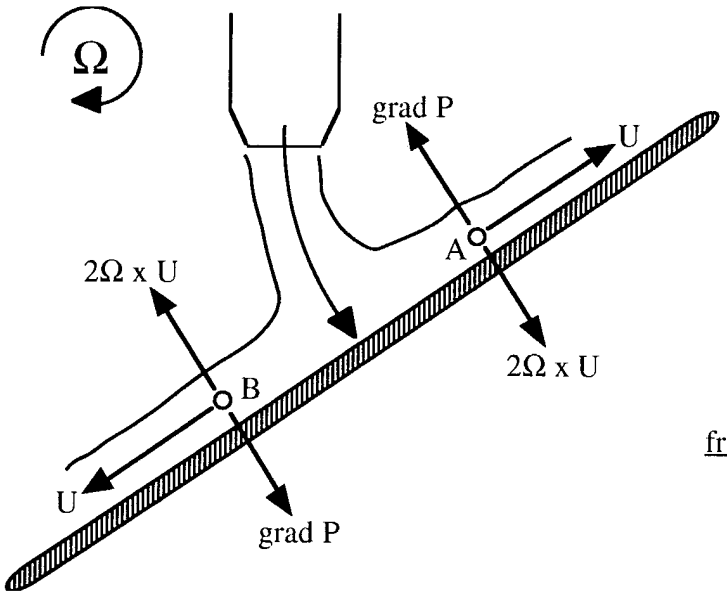

from momentum equation:

$2\Omega \times U = -(\text{grad } P)$

Figure 19. Lateral pressure gradients in wall jets

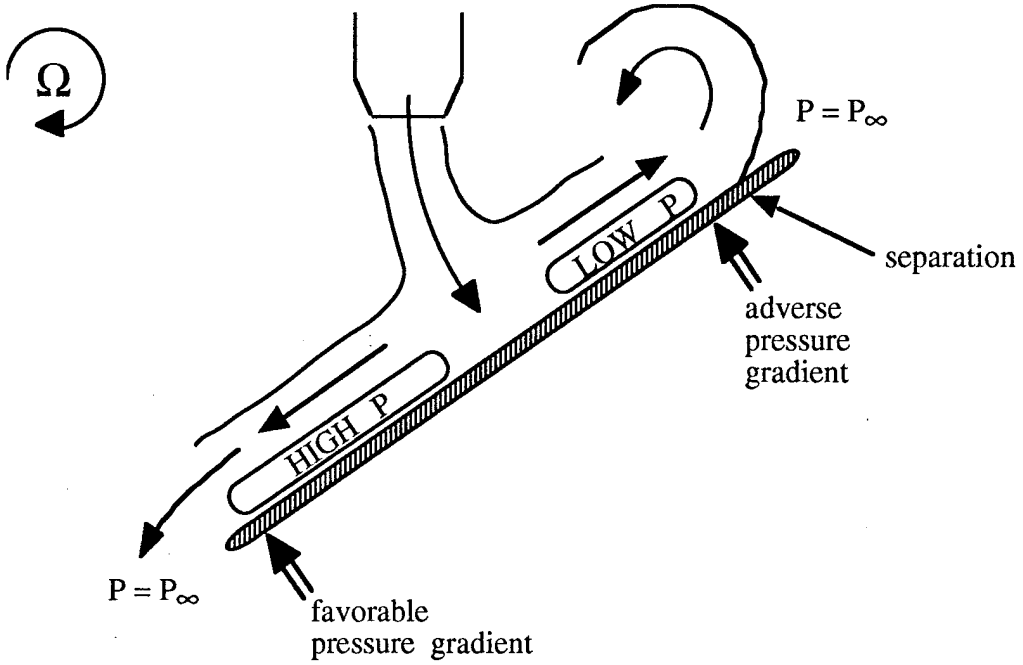

Figure 20. Effect of recovery to ambient pressure at plate edges

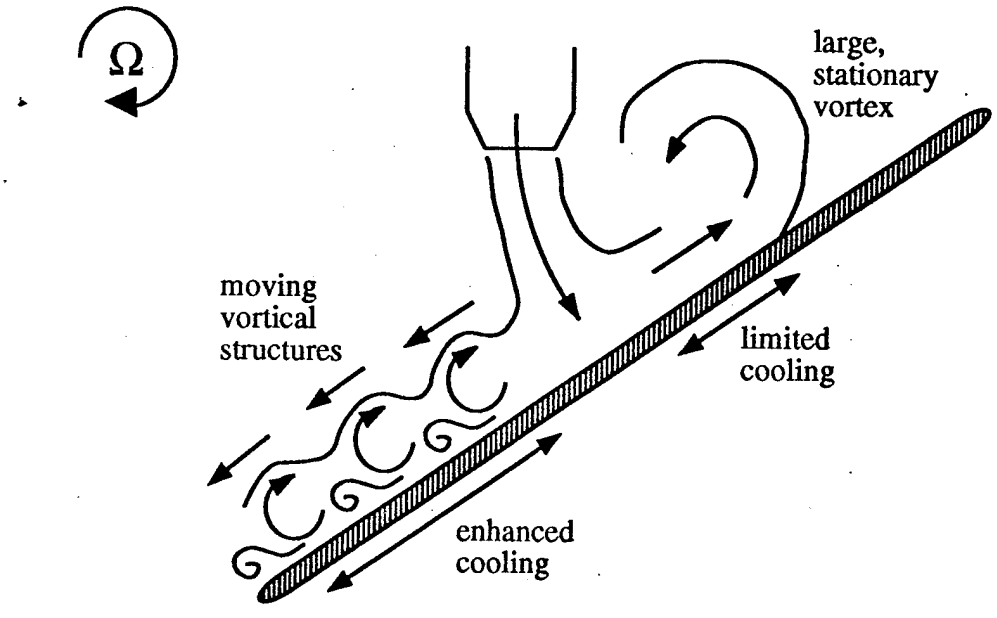

Figure 21. Implications on cooling of the impingement plate

(9a-2) Rotating Air Test

A rotating air rig for temperature/pressure measurements was also constructed and it is shown in Figure 22 (ref. 3). Its nominal speed of rotation is 3000rpm, maximum design speed is 4200rpm.

The air supply for the jet is located in the basement of a separate building and can be controlled from a panel in the laboratory using dome regulators. On its way to the test rig, the air travels through a 50 kW heater, which is used to maintain the air temperature constant throughout the experiments, then through a settling chamber and a circular contraction section. At this point, the air flow enters a 4" diameter pipe in the rotor of the test rig. A labyrinth type seal assures the flow connection between the stationary and rotating reference frames. Honeycomb inside the 4" pipe imparts rotational energy on the air and serves to spin it up to the speed of the rotating frame before it exits through the jet *nozzle* into the test section. The test section is bounded by an 18" diameter, 29" long aluminum cylinder, mounted on bearings at both its ends such that it rotates along its major axis. Inside this cylinder, or canister as it is referred to throughout this paper, is located a 16" diameter acrylic disc (also rotating) instrumented with pressure taps and thermocouples. This disc is the *i*mpingement plate and is mounted on the end of a locating shaft which can be moved axially in order to set, x, the distance between the impingement plate and the nozzle. At the downstream end of the canister, holes in the end surface allow the air to exhaust from the test section. The nozzle section, canister, impingement plate and its locating shaft are all connected and make up the rotor of the test rig which is driven by a variable speed control AC motor and a V-belt drive system. In impinging jet experiments, data is taken by pressure taps and thermocouples

mounted on the exposed surface of the impingement plate. A Scanivalve transducer mounted inside the locating shaft converts the pressure information to a voltage signal which along with the thermocouples voltages is then sent to the data collection and analysis instruments in the stationary reference frame through a 50 channel slip ring. The test rig is mounted on a frame secured to heavy steel rails and located inside an existing semi-anechoic chamber. Though this location was dictated by the outlet of the air supply in the laboratory, the anechoic chamber with its thick walls conveniently isolates the loud jet noise and the potentially dangerous high speeds of the test rig.

The rig was checked out to be operational up to 22 Hz and preliminary temperature data were obtained, but more detailed study is needed for the rig to become fully functional.

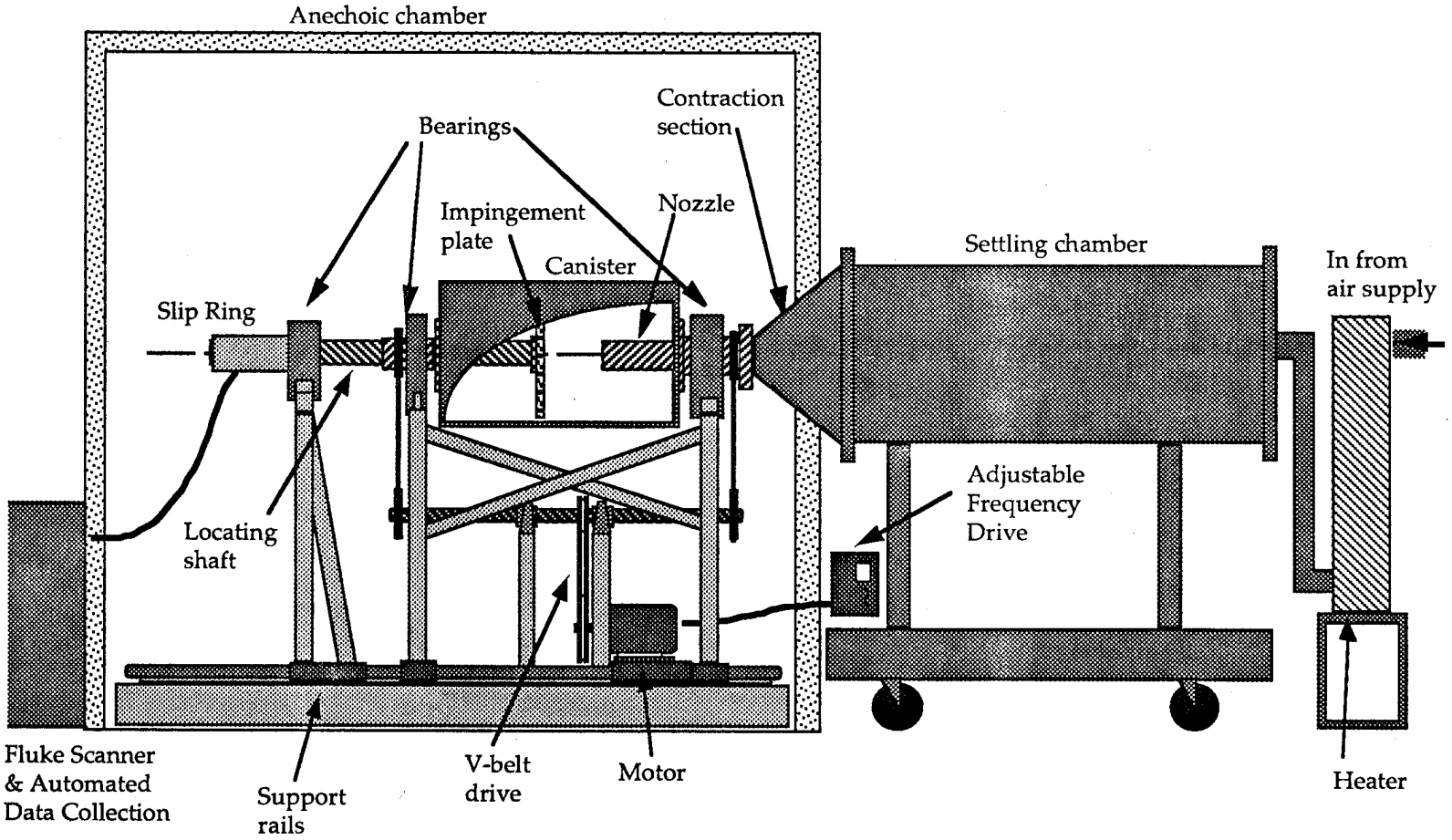

Figure 22. Rotatimg Air Tunnel.

(9b) Program B

In a low-speed water tunnel, the presence of corewise transport through the legs of a horseshoe vortex, the so-called tornado effect, has been confirmed (ref. 4). The horseshoe vortices are generated synthetically in a laminar boundary layer by several means, such as a hemispherical protuberance and secondary fluid injected through slots drilled normal to the main flow; among them, the pulsed fluid injection was found to suit our purpose best. By precise dye injection, the existence of almost straight-line trajectories inclined about 45° from the main flow direction, which correspond to the transport through the legs of horseshoe vortices, was observed and recorded. Using warm water injected directly into the core as a passive marker, this corewise transport was also verified by measuring the temperature at various points along the hairpin vortex core. The transport velocity or updraft was measured to be comparable to the freestream velocity. The details of these findings are published in "Corewise cross-flow transport in hairpin vortices-The 'Tornado effect' ", by J.P. Hagen and M. Kurosaka, *Physics of Fluids*, A **5** (12), 1993, pp.3167-3174, which is appended next.

Corewise cross-flow transport in hairpin vortices—The "tornado effect"

J. P. Hagen and M. Kurosaka
Department of Aeronautics and Astronautics, University of Washington, Seattle, Washington 98105

(Received 30 April 1993; accepted 10 August 1993)

There is increasing awareness that even in fully turbulent boundary layers, large-scale structures in the form of hairpin vortices abound. Although their implications are not all that clear at the present time, they seem to play an important role in turbulent flows. Due to the inherent unpredictability of hairpin vortices in their natural state, in the past effort has been made to generate synthetic hairpin vortices in a laminar boundary layer; from their study considerable insight into the processes underlying various features of turbulent flows has been gained. Contrary to those preceding studies where attention has been directed to the flows external to hairpin vortices, interest here is focused solely upon their *interiors*: the possible existence of cross-flow transport inside the cores of the hairpin legs. In synthetic hairpin vortices, the presence of such a corewise transport away from a wall surface, or the "tornado effect," is substantiated in a water tunnel with flow visualization techniques. The effect is also verified using heated fluid injected near the wall surface by measuring the temperature at various points along the hairpin vortex core.

I. INTRODUCTION

We propose, and confirm experimentally, a previously unexplored process of mass, momentum, vorticity, and heat transport for hairpin vortices: a phenomenon called here the "tornado effect." Before describing this, a brief background discussion on hairpin vortices in general is in order.

Many recent investigations in turbulent boundary layers have brought to light nonstochastic flow features. Among them, work by Head and Bandyopadhydy[1] seems to be the first in which convincing evidence for the presence of hairpin or horseshoe vortices populating turbulent boundary layers was offered. These vortical structures are characterized by a pair of counter-rotating "legs" inclined at 45° to the wall, joined by a "head" near the edge of the boundary layer, and growing while being swept downstream. Recent direct numerical simulations[2,3] have also reproduced, if not precisely all the features of hairpin vortices, at least some semblance of them.

Since in actual turbulent boundary layers hairpin vortices exist in large numbers and beyond easy control, attempts have been made to generate synthetic, discrete hairpin vortices in a laminar boundary layer and examine them in detail. Acarlar and Smith,[4,5] for instance, used a hemispherical protuberance mounted on a wall or fluid injection from the wall as generating devices for synthetic hairpin vortices. In either method, the vortex filaments within the oncoming boundary layer, whose axes are aligned transversely to the flow, become perturbed upwards and subsequently evolve, by mutual induction, into a train of hairpin vortices. Comparisons with turbulent flows show favorable agreement, not only in the details of vortical structures such as the counter-rotating legs, the head, and the 45° inclination, but in the overall characteristics of the near-wall region as well. For example, flow visualization by hydrogen-bubble techniques displays striking similarities between synthetic and fully turbulent hairpin vortices with regard to such well-known features as the high- and low-speed streaks and the liftup or bursting of low momentum fluid. Since these characteristics can be ascribed to induction by hairpin vortices, such vortices appear to play a crucial role in turbulent boundary layers.

These studies are, however, all concerned only with flow *outside* the cores of the hairpin vortices. Here, we turn our attention to flows *inside* the core and offer evidence of a strong current racing through the vortex core. This is much like an updraft in a tornado. Such a tornado effect has been observed previously under conditions whereby the axes of vortices such as the von Kármán vortex street and other large-scale structures[6,7] are created near, and aligned normal to, a bounding wall. (Although the no-slip condition is not a prerequisite and the existence of velocity gradients along the vortex axes is sufficient to induce the effect,[8,9] we confine our present study to the wall-vortex interaction.)

Before explaining the tornado effect in the present hairpin vortex, let us for now focus upon the aforementioned normal vortex so as to consider the effect in the simplest context. Such a normal vortex is sketched in Fig. 1, where y is the distance measured along the vortex axis from the wall, r is the radial distance from the axis, and $R(y)$ is the core radius. Assume that the flow is incompressible, the radial acceleration is negligible, and the core is in solid body rotation. Integration of the radial force balance from $r=0$ to $r=R$ with y fixed yields

$$P_c(y)=P(R)-(\rho/2)v_\theta(R,y)^2, \tag{1}$$

where $P_c(y)$ is the pressure at the center of the vortex core at position y, $P(R)$ and $v_\theta(R,y)$ are the pressure and the circumferential velocity at the outer edge of the vortex core, respectively, and ρ is the density. Since at $y=0$, $v_\theta=0$, it follows that

$$P_c(y)-P_c(0)=-(\rho/2)v_\theta(R,y)^2. \tag{2}$$

Since $v_\theta(R,y)$ increases as the distance from the wall y increases, the pressure at the vortex center $P_c(y)$ decreases: the resulting pressure gradient pumps fluid *away* from the

 0899-8213/93/5(12)/3167/8/$6.00 © 1993 American Institute of Physics

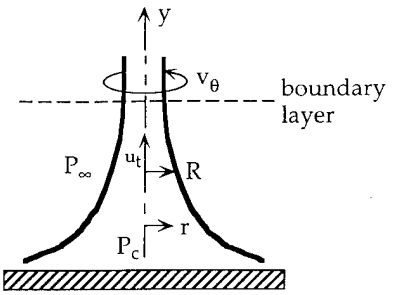

FIG. 1. Schematic showing cutaway of vortex core normal to solid boundary.

wall *through* the vortex core. This corewise transport is what is called here the tornado effect for obvious reasons.

In order to estimate roughly the magnitude of the corewise transport velocity, u_t, we ignore the effect of viscosity and simply apply Bernoulli's equation between the wall and some y position, obtaining

$$u_t \approx v_\theta. \tag{3}$$

That is, the corewise transport velocity is of the same magnitude as the rotational velocity of the vortex core.

The above argument is applicable even to the case where the vortex axis, y, is not normal to the wall. Thus the tornado effect is expected to take place through the two legs of the hairpin vortices, which are inclined 45° to the wall. This corewise transport, shown schematically in Fig. 2, should transport fluid, and hence mass, momentum, vorticity, and heat—as if through a "pipeline"—pulling them away from the near wall into the free stream in an organized and efficient manner. (A model of hairpin vortices with tornadolike structures was also suggested to be the generating cause of flow noise by Dinklæcker.[10])

The aim of the present paper is, and its scope is limited to, the substantiation of the tornado effect, or corewise transport, through the legs of hairpin vortices which are generated synthetically in a laminar boundary layer. The

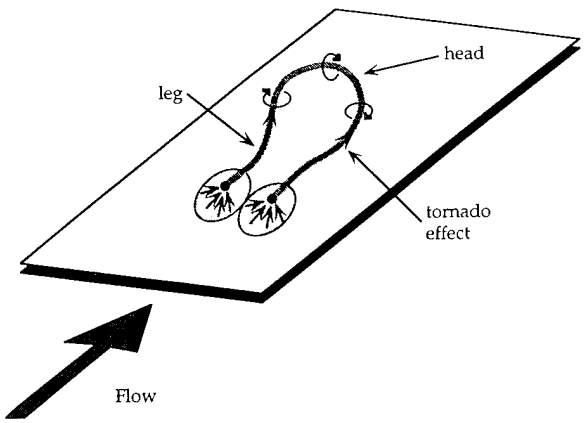

FIG. 2. Proposed view of transport through the core of a hairpin vortex.

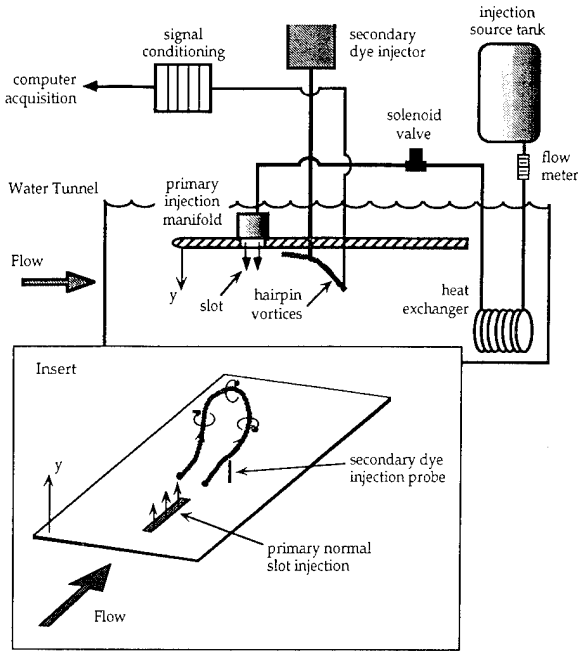

FIG. 3. Schematic of elements of hairpin vortex generation and data acquisition apparatus in water tunnel. (Note that the vertical orientation of the insert is reversed from the actual one.)

confirmation is done by two methods: flow visualization using dye and tracking of transport by passive heated tracer.

II. EXPERIMENTAL APPARATUS

As a means of generating synthetic hairpin vortices in a laminar flow, a fluid injection method similar to the one originally employed by Acarlar and Smith[5] was adopted: As shown in Fig. 3, fluid was injected through a streamwise slot in a flat plate in the direction normal to the main flow. Whenever necessary, the injection will be called the primary fluid slot injection in order to distinguish it from the secondary injection to be discussed in Secs. III and IV.

This test was carried out in the University of Washington's low-speed water tunnel facility. The test section is open channel with dimensions 0.75 m wide$\times$0.6 m deep $\times$3.0 m long. A 0.5$\times$1.0 m Plexiglas plate with an elliptical leading edge is mounted 8.0 cm below the water surface (Fig. 3). The working surface is the bottom side (thus the positive y direction is downward in the actual setup). This choice was made to ensure that when warmer fluid injection was used as a tracer (Sec. IV) to confirm the tornado effect, it can be separated from any buoyancy effects: In this arrangement, the former is expected to transport fluid downward, the latter upwards.

The slot used was 3.175 cm long and 1.27 cm wide with circular arc ends for a total slot area of 3.7 cm^2. The leading edge of the slot was located 62 cm downstream of the leading edge of the flat plate. The boundary layer thickness, δ, corresponding to the base undisturbed flow (no injection) at the leading edge of the slot is 2.5 cm, and the displacement thickness δ_* is 0.8 cm. Above the slot, on the upper surface of the flat plate, a primary injection mani-

FIG. 4. Side view of hairpin vortices generated behind slot injector with pulsing rate 0.3 Hz, injection/free-stream velocity ratio, $\zeta=0.325$, free-stream speed, $u_\infty=2.5$ cm/sec, and Reynolds number based on displacement boundary layer thickness, $\mathrm{Re}_{\delta^*}=208$.

fold, 7 cm$\times$7 cm, was installed with two opposing inlets to produce smooth flow across the entire domain of the slot.

The setup incorporated an additional provision to pulse the rate of primary fluid injection, specifically at the frequency of hairpin vortices associated with steady slot injection, hereafter referred to as the "natural" shedding frequency, in order to intensify them at resonance. In all the tests reported herein, purely on/off injection was imposed as a means of pulsing using a solenoid valve, which was found to produce the most consistent hairpin vortices.

Care was taken to avoid the generation of any parasitic vortical structures associated with transverse jets (see Fric[11]). This was achieved by keeping the ratio of slot velocity to free-stream velocity, ζ, less than one and around 0.3 (mass-flow averaged). For additional details, see Hagen.[12]

III. FLOW VISUALIZATION

As shown in Fig. 3, the water injected through the slot was dyed and placed in a pressurized source tank. From there, the fluid passed through a calibrated flow meter, a heat exchanger in the tunnel itself to equalize temperatures and eliminate any buoyancy effects, and finally a solenoid valve before being introduced into the injection manifold.

The flow pictures to follow were taken with a 35 mm still camera after approximately 30 min of settling time to allow the flow to stabilize. The pictures have been inverted upside down from that of the actual orientation. The main flow is from left to right and its free-stream velocity, u_∞, is 2.5 cm/sec.

Figure 4 is a side view of the hairpin vortex train with the primary slot injector pulsed at 0.3 Hz, the natural shedding frequency of hairpin vortices in this case. Note the downstream evolution and growth of the vortices. Their structure consists of legs turning away from the plate at about 45°, which are joined together at the head. Though not obvious from the side view, other features of hairpin vortices—a pair of parallel, counter-rotating streamwise legs—were confirmed from top and oblique views. Since the diffusivity of dye is much lower than that of vorticity (i.e., large Schmidt number), only the vortex cores have been marked.

Having thus confirmed the generation of hairpin vortices using the present setup, we proceeded to introduce secondary dye of a contrasting color into the hairpin core and investigate possible cross-flow transport. In order to inject dye directly into the core, the best method found was to place a fine secondary dye probe into the flow, positioned such as to intercept the core of the vortex on its way downstream (Fig. 3 insert). Care was taken not to inject the dye inboard of the legs; this would lead to a much more helical dye trajectory, though still in the direction away from the wall. The probe used was a glass tube with an outside diameter of 0.9 mm; no disturbance of the flow was observed. The probe was placed 4.8 δ downstream of the leading edge of the slot with the tip 0.2 δ above the plate surface.

Figure 5, a side view, shows the results of probe injection in a hairpin vortex generated by normal slot injection pulsed at 0.3 Hz. The six frames form a sequence in time, with a time span between frames of 0.3 sec, giving a total elapsed time over the sequence of 1.5 sec. The first frame shows the dyeline from the secondary dye injector (darker) just beginning to be influenced by the oncoming hairpin vortex. The dye rapidly gets pulled away from the plate along the core as the hairpin continues past the probe from the second to fifth frames. The corewise fluid seems to lie on the "trailing edge" of the hairpin, most likely due to the lag which develops as these dyed fluid particles must accelerate from zero streamwise velocity component upon injection to the speed of the rest of the fluid inside the hairpin. In the last frame of Fig. 5, the secondary dyed fluid approaching the head seems to be off a straight course. This is possibly due to the slowing down of the corewise transport, which is caused by the colliding effect of the incoming fluid from the opposite hairpin leg, in combination with the rotational effect of the head, under whose influence the approaching dye on the "trailing edge" now comes. After the passage of the hairpin vortex, the dye from the secondary probe flows more or less horizontally until it begins to be influenced by the next hairpin vortex and the process repeats itself. The top and oblique views confirm these results.

Next we examine the magnitude of the cross-flow velocity. The dye appeared to be pulled 2.5 cm vertically away from the plate, i.e., $\approx\delta$, the characteristic boundary layer thickness. Assuming an angle of 45° to the plate, this gives a total cross-flow distance of 1.41 δ. However, since the probe height above the plate was 0.2 δ, the actual cross-flow distance was only 1.13 δ. The video record shows that it takes 1.5 sec to travel this distance, giving an average corewise velocity of $u_t=0.76u_\infty$. This is in fair agreement with the estimate given by Eq. (3), if we assume that v_θ scales with the free-stream velocity.

Once carried through the legs, where does the fluid transported by the tornado effect go? Possible alternatives are "detrainment" to the free stream through the hairpin

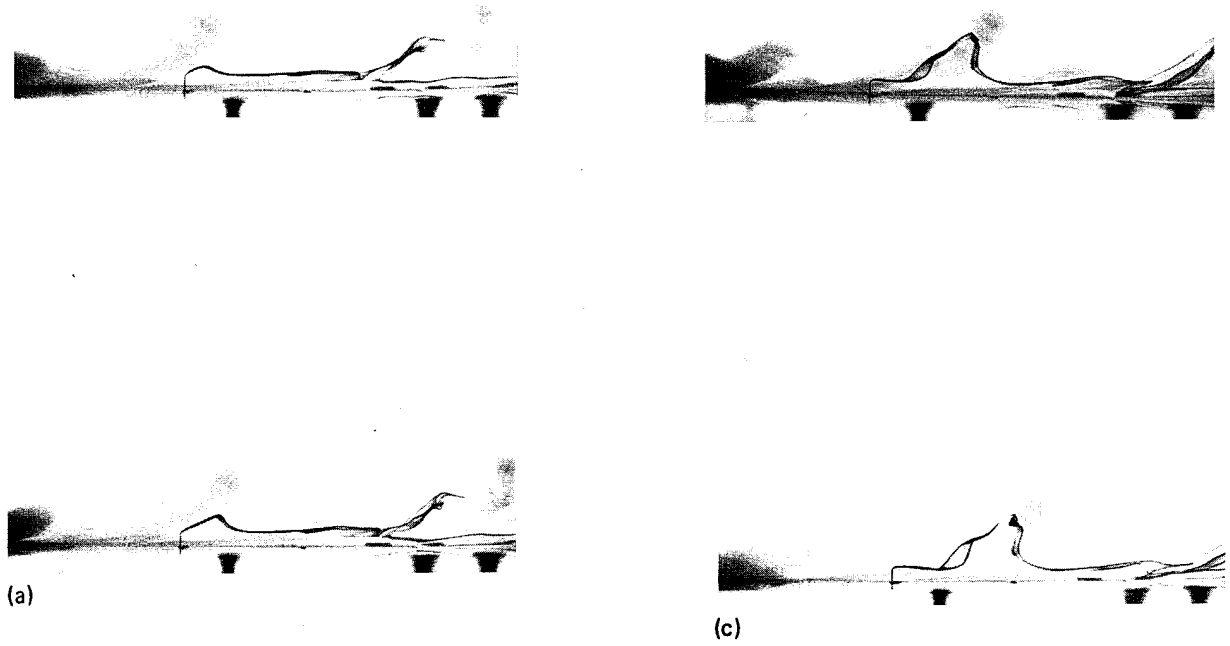

FIG. 5. Side view of cross-flow transport in 0.3 Hz pulsed slot generated hairpin vortices. $\zeta=0.325$, $u_\infty=2.5$ cm/sec, and $\mathrm{Re}_{\delta^*}=208$.

head or incorporation into part of the hairpin body; the latter would contribute to, and may very well be the cause of, its growth. The visual impressions tentatively suggest that the second hypothesis seems to be the case, although obviously this needs further substantiation.

IV. PASSIVE TRACER

Although these flow visualization results seem to offer support of cross flow through the core of hairpin vortices, a second confirmation was highly desirable. By injecting a

small amount of heated tracer fluid into the vortex core, the temperature rise could be tracked through the core. All passive tracer experiments were done utilizing normal slot injection pulsed at 0.3 Hz. The experimental setup is virtually identical to that used for flow visualization, except in this case the secondary dyed fluid from the injector probe was replaced by the fluid heated above the ambient tunnel temperature, T_∞, prior to injection.

A 0.005 in. type-K thermocouple probe was used, with the output passed to an electronic cold junction compensator, then into a Preston 8300 XWP amplifier where a 10 Hz cutoff low-pass filter was applied to eliminate high frequency noise, and the signal was amplified by a factor of 1000. This signal was then sent to a Fluke 8505A digital multimeter where it was read at a sample rate of 17 Hz by an Apple Macintosh data acquisition system. A 0.005 in. type-K thermocouple is rated by the manufacturer for 25 Hz response in still water. Thus, by sampling at nearly 20 Hz and filtering any frequency components over 10 Hz, all aliasing and most high frequency noise problems should be avoided. In the case of multiple thermocouple sensors, a 4-channel LeCroy 6810 waveform recorder was used at a sampling rate of 20 Hz to allow simultaneous measurements of all four thermocouples. This data was again filtered at 10 Hz and amplified before being collected by the computer system. The thermocouple probe was located 6.4 δ downstream from the slot leading edge, placed vertically near the edge of the boundary layer at $y=\delta$. In addition, utilizing the heat exchanger in the slot injector supply line, the temperature of the primary injection fluid could be slightly lowered. This created hairpin vortices cooler than the surrounding free stream which allowed the passage of the hairpin itself past the thermocouple probe to be easily identified.

The first runs were made without any corewise secondary injection fluid to examine the temperature structure of the hairpin vortex itself. The top plot of Fig. 6 shows time versus normalized temperature results for an experiment using slot injection with 0.3 Hz pulsing. The lower figure is a fast Fourier transform (FFT) of the time data. Note the peak at just below 0.3 Hz; this is the natural shedding frequency and the slot pulsing rate. A schematic is included as a reminder of the geometry.

In the top plot, the temperature values have been normalized by the free-stream temperature, $T_\infty=20.4$ °C in this case. The regular series of downward peaks throughout the sample period corresponds to the passage of each hairpin vortex, reflecting the colder primary injection fluid as it passed the thermocouple probe. Also, almost every downward peak contains a temperature spike whose magnitude is close to the free-stream value.

This is as expected, for with each hairpin passage there is a temperature drop due to the cooler hairpin-leg fluid, then an upward spike corresponding to the corewise transported fluid of free-stream temperature, then another drop as the trailing edge of the hairpin leg passes.

Figure 7 is the result with the hot corewise secondary injector activated. Again there is a very regular series of temperature drops indicating the passage of each hairpin

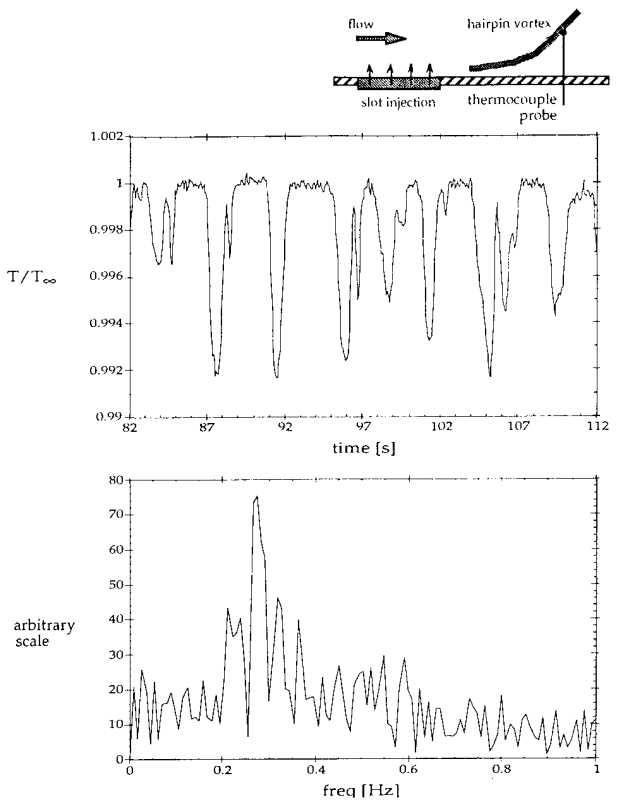

FIG. 6. Schematic, time versus temperature, and FFT results for single probe with no secondary fluid injection. Pulsing rate=0.3 Hz, $\zeta=0.325$, $u_\infty=2.5$ cm/sec, $\mathrm{Re}_{\delta^*}=208$, $T_\infty=20.4$ °C.

vortex. A corresponding sharp temperature spike is also seen with each temperature dip, indicating the passage of the hot injected fluid. Note that there is a missing upward spike in the pattern. This is due to the narrow region into which the hot fluid was gathered in the core. Any small

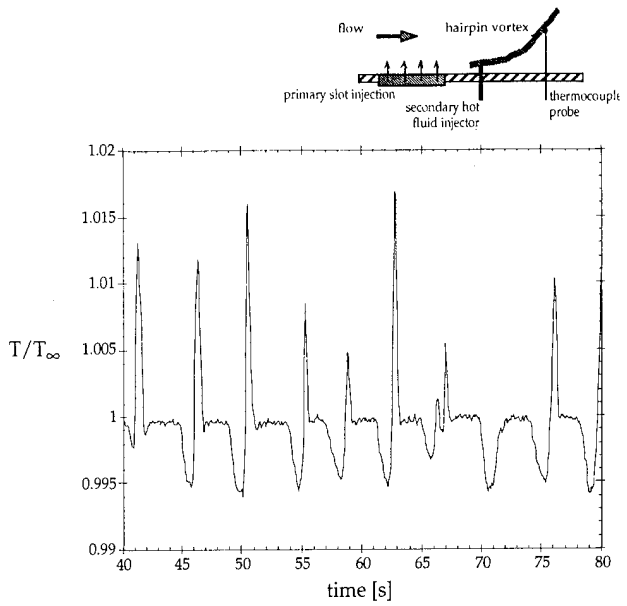

FIG. 7. View of 0.3 Hz pulsed slot results with hot corewise injection. $\zeta=0.325$, $u_\infty=2.5$ cm/sec, $\mathrm{Re}_{\delta^*}=208$, $T_\infty=20.4$ °C.

variation in the hairpin trajectory or location of fluid in the core caused it to miss the thermocouple and leave no temperature trace.

From the flow visualization results of Sec. III, the prediction is that the corewise injected fluid would lie at the trailing edge of the hairpin due to the difference in velocities between the hairpin and the injected fluid. Indeed, the time versus normalized temperature results in Fig. 7 show that the temperature rise occurs after the initial dip from the hairpin itself. The injected fluid is being pulled into the core and carried away from the plate, but near the upstream side or trailing edge; for this reason there is no second temperature dip, as was observed previously in Fig. 6. In terms of a comparison between the flow visualization results and Fig. 7, for each hairpin passage the time span between the local minimum and maximum is approximately 0.5 sec, which corresponds to a distance of about 1 cm. The is in fair agreement with the visually observed thickness of the vortex core.

As another verification, four thermocouples arranged as a probe perpendicular to the wall surface were utilized. The thermocouples were spaced 5 mm apart and situated such that the thermocouple furthest from the plate, referred to as channel 1, was at the edge of the boundary layer, 2.5 cm from the plate [see sketch inserted in Fig. 8(a)]. This put the sensor closest to the wall, channel 4, at 5 mm from the wall, which was also the height of the hot fluid injector probe above the plate. The primary slot injection fluid, pulsed at 0.3 Hz, is not cooled. Thus, if the flow were straight and horizontal, there would be a constant "warm" signal on channel 4 corresponding to the secondary hot fluid injection and not on any other channel. With primary injection activated, however, corewise spiky traces on each of the four thermocouple channels should be expected. The probe was placed far enough downstream of the corewise injector so that the heated fluid had been carried toward the head of the hairpin before it reached the temperature sensor. Thus, with channel 1 furthest from the plate, channel 2 next down, and so on, there should be a time lag between the temperature spike on each channel. Channel 1 should spike first, followed by channel 2, etc. At a hairpin angle measured to be between 45° near the head and 30° closer to the wall, and a downstream convection velocity of 0.75 u_∞ based on flow observations, our probe spacing of 0.2 δ should give a phase lag between 0.31 and 0.54 sec.

The results of Fig. 8(a) with this multiple sensor probe show that each channel does register a temperature rise with the passing of each hairpin, but the exact pattern is difficult to discern at this time scale. Figure 8(b) is an expansion of the time scale around the temperature spike marked with an arrow in Fig. 8(a) to distinguish better the phase lag between each channel. Indeed the spike in channel 1 occurs first, followed by 2, 3, and then 4. An examination of the time span between each of these peaks shows an average lag of 0.47 sec, which is in the range predicted above.

The final experimental setup was very similar to the previous four thermocouple probe, normal to the plate. In

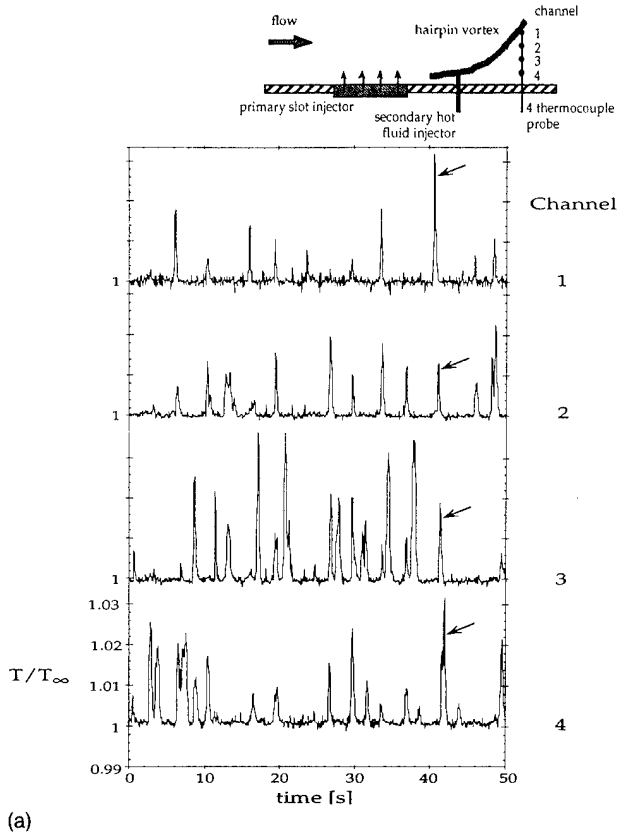

(a)

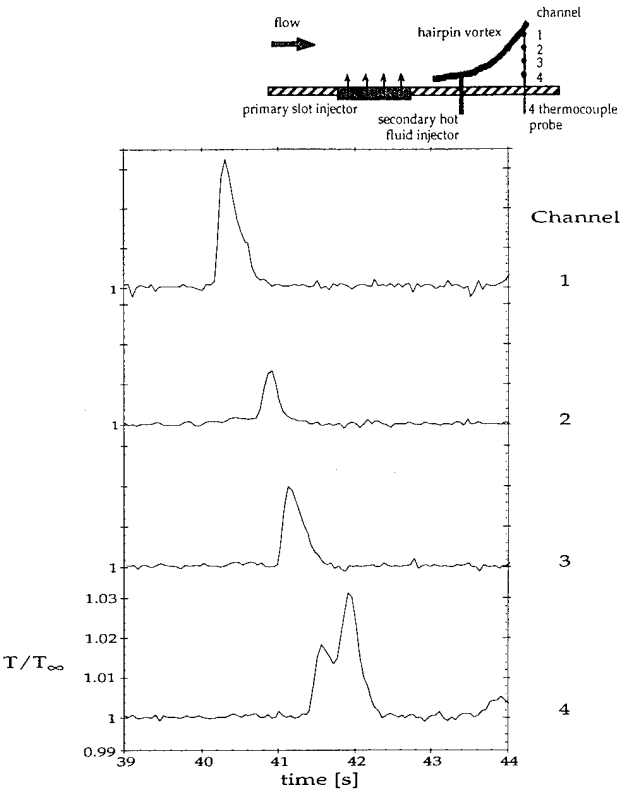

(b)

FIG. 8. (a) Plot and schematic for 90° probe with slot injector pulsed at 0.3 Hz. $\zeta=0.325$, $u_\infty=2.5$ cm/sec, $\mathrm{Re}_{\delta^*}=208$, $T_\infty=21.3$ °C. (b) Expanded plot and schematic for 90° probe with slot injector pulsed at 0.3 Hz. $\zeta=0.325$, $u_\infty=2.5$ cm/sec, $\mathrm{Re}_{\delta^*}=208$, $T_\infty=21.3$ °C

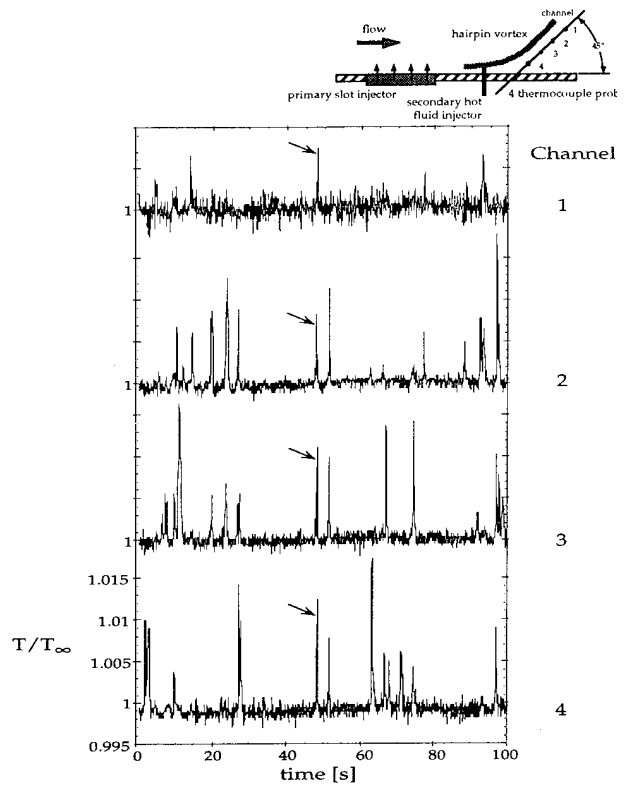

(a)

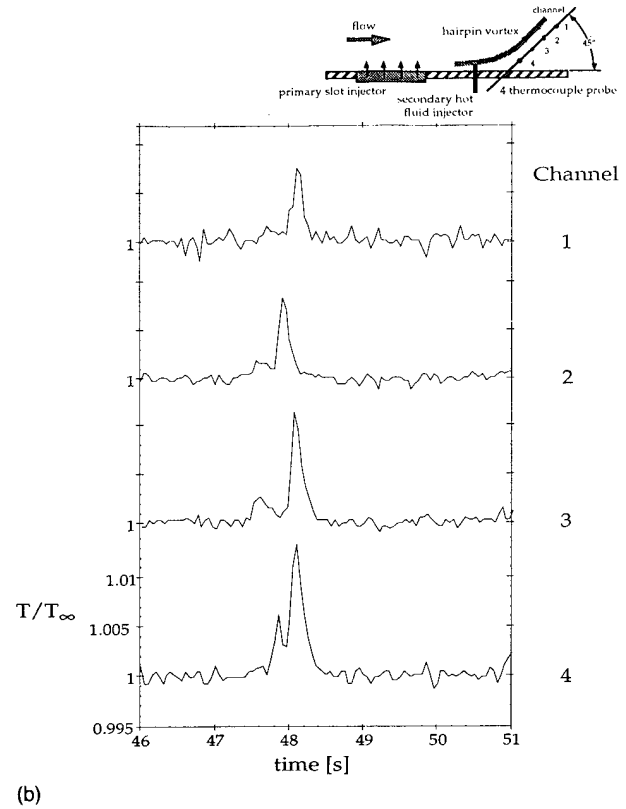

(b)

FIG. 9. (a) Plot and schematic for 45° probe with slot injection pulsed at 0.3 Hz. $\zeta=0.325$, $u_\infty=2.5$ cm/sec, $\mathrm{Re}_{\delta^*}=208$, $T_\infty=21.8$ °C. (b) Expanded plot and schematic for 45° probe with slot injection pulsed at 0.3 Hz. $\zeta=0.325$, $u_\infty=2.5$ cm/sec, $\mathrm{Re}_{\delta^*}=208$, $T_\infty=21.8$ °C.

this case the probe was inclined 45° in the downstream direction so as to place it parallel to most of the hairpin body. This geometry should eliminate the phase lag between the response of each channel in the probe. All other parameters of pulse rate and probe locations remain the same as in the previous case. Figures 9(a) and 9(b) are the results for this probe orientation. Examining the time versus temperature data with an expanded scale around the marked temperature rise in Fig. 9(b), the phase lag is seen to be more or less eliminated and the temperature spike from the hot core injection occurs at each channel virtually simultaneously, indicating cross-flow transport has occurred in the core of the hairpin vortex.

V. CONCLUSIONS

The objective and the scope of the present investigation is to confirm the presence of corewise, cross-flow transport in hairpin vortices generated in a laminar boundary layer. In hairpin vortices created by fluid injection, the results of both flow visualization and passive heated tracers did support the presence of the tornado effect in hairpin legs. The legs act like inclined mini-tornados sweeping over the plate and transporting the mass, momentum, vorticity, and heat directly from the wall to the free stream.

It is interesting to note the similarities of time-traces between the present Figs. 8(a) and 8(b) for a *laminar* flow with Fig. 12 of Chen and Blackwelder[13] for a fully *turbulent* flow. Both were obtained with multisensored probes placed normal to the wall but in the latter no intentional injection of the heated fluid to the core was attempted. Instead the flat plate was heated and the hot spikes observed by them appear to be interpretable as caused by the tornado effect.

Once substantiated, this corewise transport would act like "pipe flow," carrying heat directly from the wall to the free stream without interruption. The tornado effect might indeed be a powerful transport process.

ACKNOWLEDGMENTS

The authors would like to thank D. C. Aronstein, M. D. Fox, and M. J. Aarnio for their advice and suggestions throughout the course of these experiments.

This work was supported by the Air Force Office of Scientific Research under Grant No. AFOSR-91-0195 under the technical monitoring of Major Daniel B. Fant.

[1] M. R. Head and P. Bandyopadhydy, "New aspects of turbulent boundary layer structure," J. Fluid Mech. **107**, 297 (1981).

[2] P. Moin and J. Kim, "The structure of the vorticity field in turbulent channel flow. Part 1. Analysis of instantaneous fields and statistical conditions," J. Fluid Mech. **155**, 441 (1985).

[3] P. R. Spalart, "Direct simulation of a turbulent boundary layer up to $R_\theta=1410$," J. Fluid Mech. **187**, 61 (1988).

[4] M. S. Acarlar and C. R. Smith, "A study of hairpin vortices in a laminar boundary layer. Part 1. Hairpin vortices generated by a hemispherical protuberance," J. Fluid Mech. **175**, 1 (1987).

[5] M. S. Acarlar and C. R. Smith, "A study of hairpin vortices in a laminar boundary Layer. Part 2. Hairpin vortices generated by fluid injection," J. Fluid Mech. **175**, 43 (1987).

[6] M. Kurosaka, W. H. Christiansen, J. R. Goodman, L. Tirres, and R. A.

Wohlman, "Crossflow transport induced by vortices," AIAA J. **26**, 1403 (1988).
[7]M. M. Koochesfahani, "Vortical patterns in the wake of an oscillating airfoil," AIAA J. **27**, 1200 (1989).
[8]L. Tirres, "A study of flows behind bluff bodies immersed in a sheared flow," M. S. thesis, University of Tennessee Space Institute, 1988.
[9]R. K. Cohn and M. M. Koochesfahani, "Effect of boundary condition on axial flow in a concentrated vortex core," Phys. Fluids A **5**, 280 (1993).
[10]A. Dinklæcker, "Play tornado-like vortices a role in the generation of fluid noise?," in *Mechanics of Sound Generation in Flows,* edited by E. A. Muller, Joint Symposium of IUTAM/ICA/AIAA, Gœttington, Germany (Springer-Verlag, Berlin, 1979).
[11]T. F. Fric, "Structure in the near field of the transverse jet," Ph.D. thesis, California Institute of Technology, 1990.
[12]J. P. Hagen, "Hairpin vortex induced crossflow transport," M. S. thesis, Department of Aeronautics and Astronautics, University of Washington, 1992.
[13]C. P. Chen and R. F. Blackwelder, "Large-scale motion in a turbulent boundary layer: a study using temperature contamination," J. Fluid Mech. **89**, 1 (1978).

Concurrently, unsteady heat transfer gauges necessary for the direct confirmation of the tornado effect in air have been developed (ref. 5). The basic operating principle of the gage is to use, for time-accurate temperature measurement, the rapid temperature dependent response of the electrical resistance of a thin platinum film deposited on Pyrex glass; the function of the latter to amplify the magnitude of the temporal response of the platinum film. The detailed specification of the gauge is as follows: the active gauge area is 1/8" long by 2 mm wide. The normal room-temperature resistance is 50 W, indicating a film thickness of less than one micron. The theoretical response of the gauge is therefore in excess of 100 kHz, which is more than sufficient for the present purpose. Head wires are brought in from the rear of the gauge body to allow for mounting flush with a wall.

The key result is shown in Figures 24 and 25.

Here the frequency spectrum for the pressure and heat transfer signals is plotted on the top of the figures, with a schematic underneath showing the relative position of the instrumentation and the hairpin vortex. On the bottom of each figure a snapshot of the hairpin vortices from the flow visualization, along with sketches of the slot and gage position, is provided. The test condition for this data are as follows: freestream velocity=2.4 m/s and the injection velocity =0.23 m/s.

In Figure 24, strong peaks in the frequency spectra of both the pressure signal and the heat transfer signal is observed, at a frequency of 46 Hz. This frequency is close to the expected range. This case corresponds to that of the gages lying directly in the path of the hairpin vortex legs.

Figure 24 is the counterpoint of Figure 23. Here the gages are located outside of the path of the hairpin vortex legs. It is observed that the pressure signal is gone, and although there is still a peak in the heat transfer signal, it is more than an order of magnitude weaker.

The conclusion drawn from the above is that the 'tornado' effect does increase the heat transfer from a heated wall and may be exploited for enhanced heat transfer in convected cooling. It also has implications in film-cooling, a scheme where coolant is injected through a slot in much the same way as the present injection method.

In ref. 6, an attempt was made to enhance, by acoustic excitation, the hairpin vortical structures and hence the tornado effect. The corewise transport appears to be enhanced but more study is needed to draw definitive conclusions.

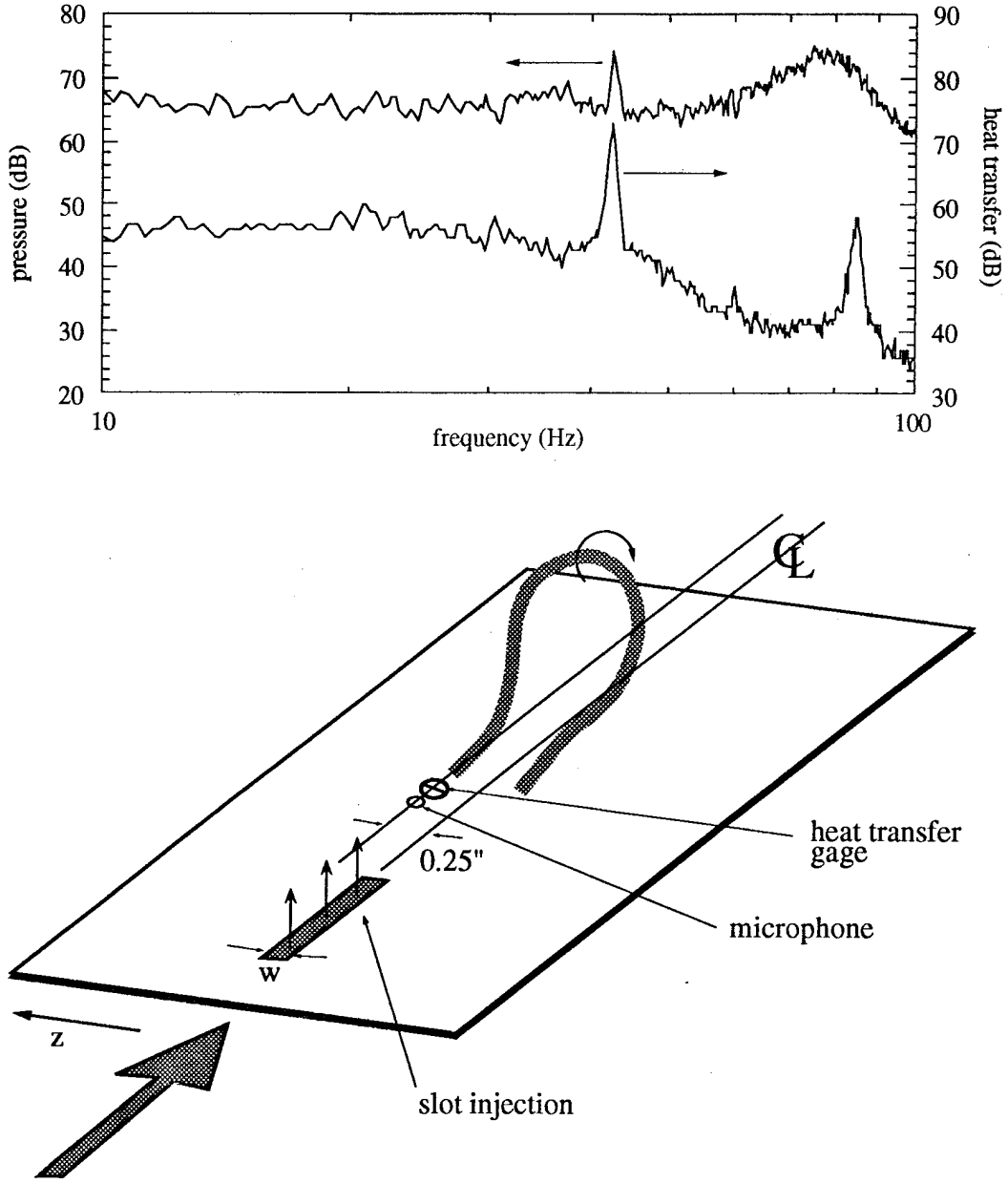

Figure 23. Heat transfer and pressure measurements:

the gages are located underneath the hairpin leg trajectory.

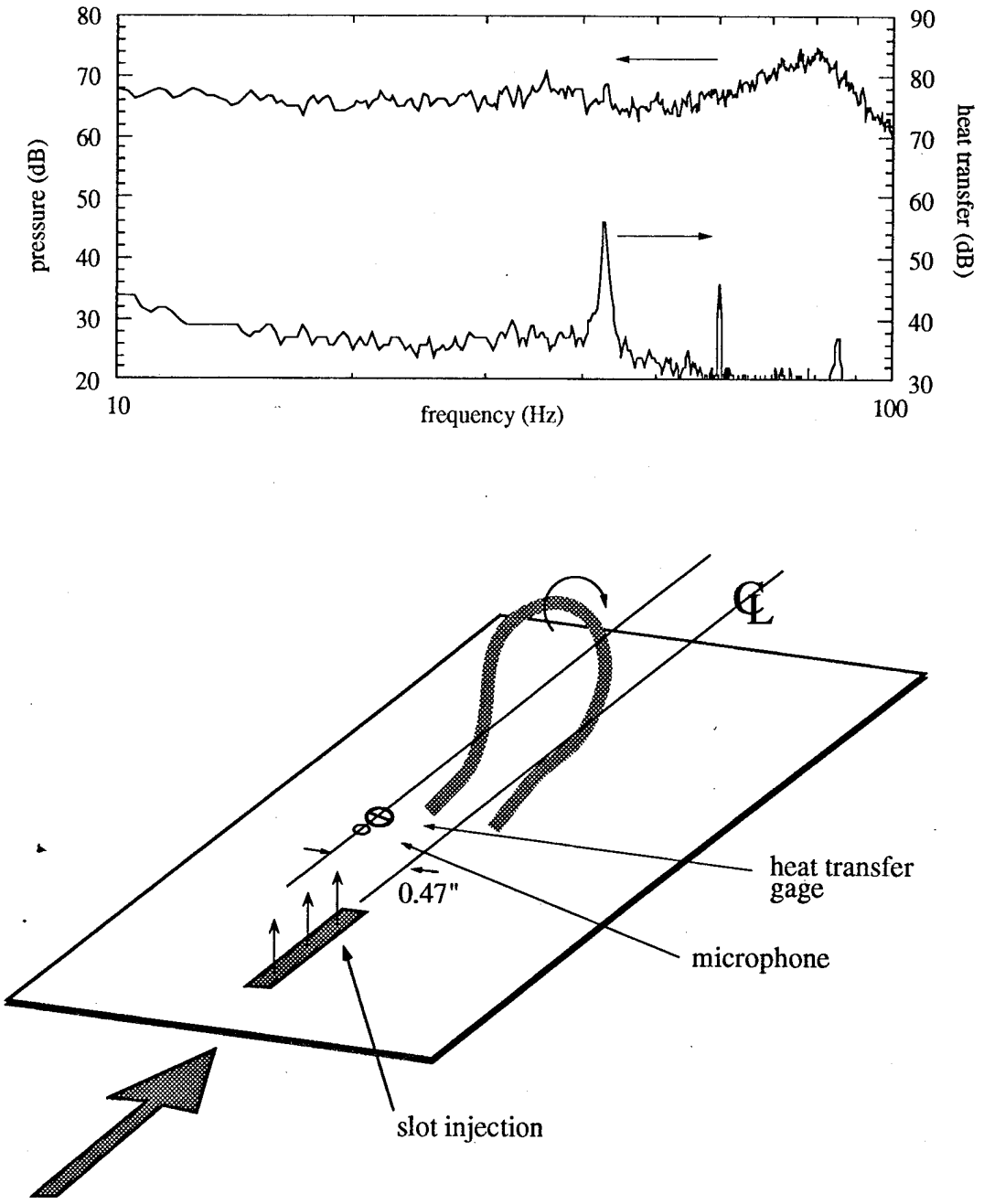

Figure 24. Heat transfer and pressure measurements:

the gages are located outside the hairpin leg trajectory.

(9c) References

1. "Effects of Rotation on Impinging Jets for Turbine Cooling",

David. C. Aronstein, Ph.D. Thesis, Department of Aeronautics and Astronautics,

University of Washington, Seattle, WA, 1994.

2. "Effect of Boundary on Impinging Jets in a Rotating System",

Stanley Hsu, MS Thesis, Department of Aeronautics and Astronautics,

University of Washington, Seattle, WA, 1993.

3. "Design of a High Speed rotating Air Jet Facility for Impingement Cooling

Studies", Philippe C. Poutissou, MS Thesis, Department of Aeronautics

and Astronautics, University of Washington, Seattle, WA, 1994.

4. "Hairpin Vortex Induced Crossflow Transport", Jeffery P. Hagen, MS Thesis,

Department of Aeronautics and Astronautics, University of Washington, Seattle,

WA, 1992.

5. "The Effect of Large-Scale Vortical Structures on the Heat Transfer

from the Surface", Michael D. Fox, Ph.D. Thesis,

Department of Aeronautics and Astronautics, University of Washington,

Seattle, WA, 1994.

6. "A Flow-Visualization Study of Acoustically Enhanced Hairpin Vortices"

Stephen A. Whyte, MS Thesis, Department of Aeronautics and Astronautics,

University of Washington, Seattle, WA, 1993.